Does Brownification and Iron Affect Microbial Communities and Mixotrophic Activities? Experiences From a Mesocosm Experiment

Anna Grytaas

A master thesis in microbiology

2020

Department of Biological Sciences

UNIVERSITY OF BERGEN

i Abstract

In one millilitre of seawater there is on average approximately 10^6 microbial cells, and these are largely responsible for nearly half of all primary production on Earth. Mixotrophic microorganisms are ubiquitous in the photic zone of the ocean yet their role has long been unclear. Marine mixotrophs are, as all marine organisms, expected to be affected by the current climate changes. Increased temperatures are expected to increase brownification of lakes and coastal waters due to more precipitation causing higher input of dissolved organic carbon (DOC). The darker water is in turn hypothesised to increase phagotrophy in mixotrophs due to lower availability of light, which is needed to perform photosynthesis. Increased availability of dissolved iron (dFe) has been observed in relation to increased input of DOC. My main hypotheses were that brownification and increased dFe concentrations lead to changes in the microbial community composition, that brownification promotes higher percentages of mixotrophic plankton, and that altered dFe concentrations affect these percentages. To test these hypotheses, samples from a mesocosm experiment were examined through flow cytometry by enumerating different groups and species and, using the probe LysoTracker, investigating how many phototrophs performed phagotrophy. Here I show that brownification did change the composition of the microbial community but did not lead to higher percentages of mixotrophic organisms. Addition of dFe did not affect composition nor mixotrophic percentages. Among the groups accounted for in this experiment, brownification led to increased abundances of autotrophic picoeukaryotes and bacteria, and decreased abundances of autotrophic nanoeukaryotes (ANEs). Brownification also led to decreased percentages of mixotrophic ANE cells. Though addition of dFe was expected to induce a bloom of the coccolithophore *Emiliania huxleyi*, no effect was observed in any of the studied groups. Some ANEs were pictured through confocal microscopy and shown to have unspecific staining from LysoTracker. The factors controlling mixotrophy in microbial communities, especially in relation to climate change, are yet to be understood. As this and similar studies show, a change in the microbial communities is expected to happen due to ongoing climate change. Understanding these effects is important to understand how whole marine communities will change. This is just one of many new studies in this study area, and there is much yet to explore before a clearer understanding of what will happen is reached.

ii Acknowledgements

This work was supported by MIXsTRUCT (Research Council Norway, project #280414).

My time with the microbiology group at BIO has been wonderful and full of learning and kindness. First and foremost, I must express my gratitude to my incredible supervisors Aud Larsen, Bernadette Pree, and Kyle Mayers, who have all been very kind and patient with me, and have helped me get back on track when I have been stuck during the writing process. I especially appreciate Bernadette taking time out of her days for me even as she is at home with a new-born, as well as her guidance in the lab. I also have to acknowledge the team of the BIPWeb project (https://coccosphere.es/bipweb/), led by María Segovia, for setting up the mesocosm project and doing the work involved with sampling. With the help of Hege Avsnes Dale at the Molecular Imaging Centre (MIC, University of Bergen) I was able to obtain micrographs of cells, so a big 'thank you' to her. In the flow cytometry lab, Elzbieta Petelenz has been very helpful any time I have questions and always makes sure everything is in order, which I am grateful for. Lastly, I must give appreciation to my amazing friends and family members who have supported me these past two years, and to my beautiful and cuddly cats who are always there for me after long and stressful days.

iii Table of content

i Abstract 1
ii Acknowledgements 2
iii Table of content 3
iv Abbreviations and terms 5
1 Introduction 6
1.1 Marine microorganisms 6
1.2 Climate change and mixotrophy 9
1.3 Studying mixotrophic microbes 10
1.4 Knowledge gaps 12
1.5 Objectives 13
2 Materials and methods 15
2.1 Mesocosm setup 15
2.2 Flow cytometry 16
2.3 Data analysis 19
2.4 Statistical analysis 19
3 Results 20
3.1 Abundances of microbial groups 20
3.1.1 Autotrophic nanoeukaryotes 20
3.1.2 Cryptophytes and *Emiliania huxleyi* 21
3.1.3 Autotrophic picoeukaryotes 22
3.1.3 Bacteria 23
3.1.4 Heterotrophic nanoflagellates 24
3.2 Percentages of LysoTracker positive cells 25
3.2.1 Autotrophic nanoeukaryotes 25
3.2.2 Cryptophytes and *Emiliania huxleyi* 26
3.2.3 Autotrophic picoeukaryotes 27
4 Discussion 29
4.1 Effects of brownification on the composition of the community 29
4.1.1 Succession patterns of the different groups 29
4.1.2 Was there a difference between treatments? 31
4.2 Effects of brownification on percentage of mixotrophs 33
4.2.1 Development of percent LysoTracker positive cells 33
4.2.3 Was there a difference between treatments? 36

4.3 Effects of iron addition 37
4.4 The LysoTracker method 39
4.5 Conclusion 42
4.6 Future Work 43
References 45
Appendix A: Methods 53
A.1 Flow cytometry settings 53
A.2 F_v/F_m 54
A.3 Confocal microscopy 54
Appendix B: Results 55
B.1 F_v/F_m 55
B.2 Effect of iron treatment 56
B.2.1 Abundances of microbial groups 56
B.2.2 Percentages of LysoTracker positive cells 61
B.2.3 F_v/F_m 63

iv Abbreviations and terms

ABBREVIATIONS

ANE	Autotrophic nanoeukaryote
APE	Autotrophic picoeukaryote
Bro	Brownification
dFe	Dissolved iron
DOC	Dissolved organic carbon
DOM	Dissolved organic matter
FLB	Fluorescently labelled bacteria
HNF	Heterotrophic nanoflagellate
N	Nitrogen
P	Phosphorus
POM	Particulate organic matter
SE	Standard error

TERMS

Autotrophy	Nutritional process where CO_2 is reduced and assimilated into cell material. Includes phototrophs (through phototrophy) and chemolithotrophs (through chemosynthesis).
Constitutive mixotrophs (CMs)	Organisms that perform phagotrophy and have an inherent capacity of phototrophy. (See **Box 2**)
Eutrophic	Rich in organic and mineral nutrients.
Heterotrophy	Nutrition involving use of organic compounds as a carbon source.
Meso-	Prefix indicating an organism size of >200 µm.
Micro-	Prefix indicating an organism size of 20-200 µm.
Microbe	Microorganism, organism too small to be seen by the naked eye.
Mixotrophy	Nutrition involving both autotrophy and heterotrophy. (See **Box 2**)
Nano-	Prefix indicating an organism size of 2-20 µm.
Non-constitutive mixotrophs (NCMs)	Organisms that perform phagotrophy and acquire a capability for phototrophy by consuming phototrophic prey. Prey can be specific (SNCMs) or non-specific (general; GNCMs). (See **Box 2**)
Oligotrophic	Poor in nutrients.
Phagotrophy	A form of heterotrophy that involves engulfing a particle to bring it into the cell to be digested.
Phototrophy	A form of nutrition that involves conversion of light energy into ATP that is used in cellular processes. Often combined with autotrophy (photoautotrophy) to fix CO_2 using light energy.
Pico-	Prefix indicating an organism size of 0.2-2 µm.
Plankton	Organisms suspended in the water column that are unable to resist water currents.

1 Introduction

1.1 Marine microorganisms

Microorganisms, organisms too small to be seen by the naked eye (Madigan et al., 2019), have been observed for several centuries. Their discovery is credited to Antonie van Leeuwenhoek in the second half of the seventeenth century (The Editors of Encyclopaedia Britannica, 2019). It was only towards the end of the twentieth century, with new technological advances, that studying marine microorganisms entered mainstream science, and it is still a fast-growing area of research (Munn, 2011).

The oceans cover 71% of the surface of the Earth and contain 97% of the water on the planet (Munn, 2011). In one millilitre of seawater there is, on average, approximately 10^6 microbial cells (Madigan et al., 2019). Marine environments comprise a great variety of microorganisms: bacteria, archaea, eukaryotic microbes, as well as viruses (Munn, 2011). The eukaryotic microbes include a wide variety of organisms at several levels in the food web, including smaller phototrophic microbes like haptophytes, heterotrophic flagellates like dinoflagellates, and ciliates that graze on other microbes (Munn, 2011).

The oceans perform nearly half of all primary production on Earth, of which the microorganisms are responsible for a large proportion (Field, Behrenfeld, Randerson, & Falkowski, 1998). Carbon dioxide (CO_2) is used by autotrophic organisms to create particulate organic matter (POM) and dissolved organic matter (DOM). This can then be taken up by small heterotrophic organisms, that in return can be eaten by larger heterotrophs (Munn, 2011). The processes in which carbon is transferred between the atmosphere, the ocean, and marine organisms, is collectively called the biological carbon pump (Mitra et al., 2014). In this cycle, CO_2 is incorporated into cell material by phototrophs, and these organisms are either eaten by heterotrophs that produce CO_2, or they die, break down to POM, and sink to the seabed (Munn, 2011). The POM can be consumed by heterotrophs like heterotrophic bacteria in the lower ocean or seabed (Munn, 2011). Models of the biological pump highlights the importance of marine microorganisms and shows how all marine life depends on the production of the autotrophs.

Since marine microorganisms were discovered, scientists have worked to understand interactions between them and their environment. In 1983 the model of the microbial loop was introduced to the marine food web (Azam et al., 1983) (**Box 1**, **Fig. 1**). The goal was to explain the cycling of DOM, in which microorganisms have important roles. In fact, about half of the

organic carbon fixed by phototrophs goes through the microbial loop, not the classic simple food chain (Munn, 2011). This model, although it has continuously developed over time with new discoveries, focuses on the traditional concept that microorganisms are either "phytoplankton" that are autotrophic and perform primary production, or "zooplankton" that are heterotrophic and perform secondary production (Flynn et al., 2013; Stoecker et al., 2017). This is based on the classification of macroorganisms on land, with "phytoplankton" resembling plants on land and "zooplankton" resembling land-living animals (Flynn et al., 2013). Of course, even among macroorganisms there is not always a clear line of distinction between the two. For example there is the carnivorous plant genus *Drosera* and the photosynthetic green sea slug *Elysia chlorotica* (Adamec, 1997; Baumgartner, Pavia, & Toth, 2015). In microorganisms the line between these is even less defined, and many are in fact mixotrophic – they can act as both "phytoplankton" and as "zooplankton" (**Box 2**).

BOX 1 | The microbial loop in the marine food web

Models of the marine food web are often very simplified, with few levels and interactions. While many include more complex interactions of macroorganisms, most do not include interactions of microorganisms beyond "zooplankton" consuming "phytoplankton" or "algae". As the importance of microorganisms in the oceans has become more recognised, new models have been introduced that include the microbial loop, which was first modelled by Azam et al. (1983) (**Fig. 1**). This model includes bacteria, autotrophic and heterotrophic flagellates, microzooplankton (heterotrophic plankton in the size range 20-200 µm, for example ciliates), mesozooplankton (heterotrophic plankton that are >200 µm, for example copepods), and often viruses. It shows much more complex interactions at the microbial stage of the food web, and emphasises the importance of dissolved organic matter (DOM) (Munn, 2011).

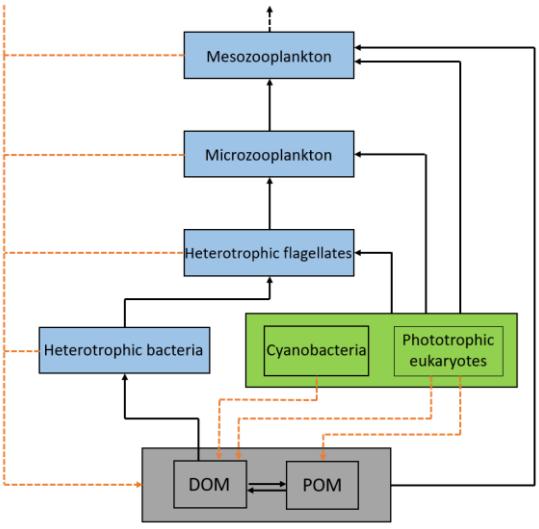

Figure 1. Model of the microbial loop in the marine food web, adapted from Azam et al. (1983). Full lines show transfer of material to the next trophic level. Dashed orange lines show transfer of material to the pool of dissolved and particulate organic matter in the oceans. Dashed black arrow at the top indicates transfer to higher trophic levels. Green squares indicate primary production and blue squares indicate heterotrophic organisms. Note that not all interactions are included here, and mixotrophic plankton will be able to act as both phototrophic plankton and heterotrophic plankton in this web at the same time. DOM = dissolved organic matter, POM = particulate organic matter.

Even though the prevalence and importance of marine mixotrophic microorganisms are beginning to be recognised, there are so many different definitions of what a mixotroph is (e.g. Godrijan, Drapeau, & Balch, 2020; Heifetz, Förster, Osmond, Giles, & Boynton, 2000; Sanders,

BOX 2 | Mixotrophy

Mixotrophy has been observed for over 100 years (Biecheler, 1936; Pascher, 1917), but only recently has the importance and prevalence of mixotrophy in aquatic environments been realised (Flynn et al., 2019; Mitra et al., 2016). There have been many attempts at defining mixotrophy, and the definition can vary depending on the field of study. Traditionally, mixotrophy referred to the acquisition of alternate forms of carbon, but now also includes acquisition of nitrogen (N), phosphorous (P), trace elements, trace nutrients, and energy (Stoecker, Hansen, Caron, & Mitra, 2017). Using different definitions, it can include everything from the uptake of dissolved organic carbon (DOC) to symbioses (Stoecker et al., 2017).

Generally, phagotrophy (uptake of nutrients in particulate form) provides nutrients like N and P, while photoautotrophy provides carbon via photosynthesis (Anderson, Charvet, & Hansen, 2018; Mitra et al., 2014). Mixotrophy exists in both the groups typically referred to as "phytoplankton" and those in the photic zone considered to be "microzooplankton" (Mitra et al., 2016). At first, mixotrophy in photoautotrophic organisms was considered to be important for uptake of nutrients primarily in oligotrophic waters, but its importance in eutrophic waters has also been recognised (Burkholder, Glibert, & Skelton, 2008). Furthermore, mixotrophy has been described in both marine and freshwater, indicating that this is a widespread strategy (Sanders, 1991).

Mitra et al. (2016) defined mixotrophs by dividing the planktonic protists into four ecological groups: (i) phagoheterotrophs with no phototrophic ability, (ii) photoautotrophs with no phagotrophic ability, (iii) constitutive mixotrophs (CMs) – phagotrophs with an inherent capacity for phototrophy, and (iv) non-constitutive mixotrophs (NCMs) that acquire their phototrophic capacity by ingesting prey that can be either specific (SNCM) or general (GNCM). These are ecophysiologically based functional groups, based on how the organisms acquire energy and nutrients.

When research began to focus more on mixotrophy, it was at first considered to be rare (e.g. Bird & Kalff, 1986; Sanders & Porter, 1988). Over time more and more species were discovered to be mixotrophic, and now it is known that mixotrophy is common in eukaryotic protists in the photic zone (e.g. Hartmann et al., 2012; Jeong et al., 2010; Pitta & Giannakourou, 2000; Sanders & Gast, 2012; Unrein, Massana, Alonso-Sáez, & Gasol, 2007; Zubkov & Tarran, 2008). Flynn et al. (2013) argues that photosynthetic protists should in fact all be assumed to perform mixotrophy, as this appears to be the norm rather than the exception. The only group of photosynthetic protists assumed to be strictly phototrophs is the diatoms (Flynn et al., 2013).

Flynn et al. (2013) presents the idea that photosynthetic protists can be placed on a continuum, with strict phototrophs and strict phagotrophs as the extremes (**Fig. 2**). This allows any mixotrophs to be placed anywhere in between. Based on their contribution to primary and secondary production they will be closer to the strict phototrophs, which only perform primary production, or the strict phagotrophs, which only perform secondary production. This continuum thus highlights the fact that primary and secondary production is in fact possible in one cell, and that the level of mixotrophy can change over time for a single cell.

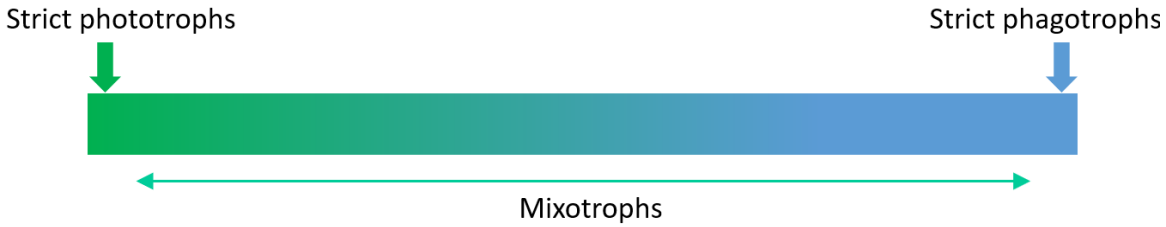

Figure 2. Illustration showing the scale of mixotrophy, from strict phototrophs at one end to strict phagotrophs at the other. All species placed between will be mixotrophic to some degree. Adaptation of figure by Flynn et al. (2013).

1991), making it difficult to compare studies and draw conclusions. Another challenge is that much of the existing science on marine microorganisms has assumed that they fit into the dichotomy and are not mixotrophs (see Flynn et al., 2013 and references therein), which could affect how we understand them today.

1.2 Climate change and mixotrophy

The ongoing climate change has received increasing focus over the last years and decades, both in scientific communities and in the general public. It is a complex mechanism with many effects. These include increasing temperatures both on land and in the oceans, increasing precipitation in the Northern Hemisphere, ocean acidification, decreasing mass of ice sheets, increasing extreme weather, and rising sea levels (IPCC, 2014). These effects in turn lead to other changes, for example in marine communities, stratification, and primary production (IPCC, 2014; Walther et al., 2002).

It is expected that the ongoing climate change will affect the composition of marine microbial communities (Harley et al., 2006). Increasing runoff from land and rivers due to enhanced precipitation affects coastal waters by increasing the amounts of dissolved organic carbon (DOC) and suspended minerals, which causes brownification and thus a decrease in the light penetration in the water (Aksnes et al., 2009; S. Larsen, Andersen, & Hessen, 2011; Pozdnyakov et al., 2007). Other factors seem to be involved in the process of brownification, though many are still debated. For example, Kritzberg and Ekström (2012) argued that iron accounts for a significant portion of the variation in water colour. They theorised that an increase in concentrations of dissolved iron (dFe) is controlled by similar processes to those controlling increases in DOM and POM. Nitrogen (N) levels in the oceans are expected to increase, both due to natural causes and agricultural runoff containing fertilizer (Randall & Mulla, 2001). This could cause the usually N-limited systems to become phosphorus (P)-limited (Cotrim da Cunha, Buitenhuis, Le Quéré, Giraud, & Ludwig, 2007; Munn, 2011). Increased input of dFe could also affect microbial communities, as iron is an essential micronutrient for growth of phototropic microbes due primarily to its central role in photosynthesis (Behrenfeld & Milligan, 2013). The increasing nutrient input will likely lead to more coastal areas becoming eutrophic (Burkholder et al., 2008), and is expected to increase phototrophic activity (Jickells, 1998).

The change in light attenuation is expected to favour mixotrophs over strict phototrophs. This is because they are not as dependent on light, and because they do not have to directly compete

for inorganic P with the bacteria (Jones, 2000). The ongoing climate change also makes the oceans warmer, which will likely favour mixotrophic phototrophs over strict phototrophs (Cabrerizo, González-Olalla, Hinojosa-López, Peralta-Cornejo, & Carrillo, 2019; Urrutia-Cordero et al., 2017). This is expected due to a predicted increase in bacteria (Urrutia-Cordero et al., 2017), as well as the limitation of photosynthetic rates due to low light and higher temperatures (Wilken, Huisman, Naus-Wiezer, & Van Donk, 2013). The expected favouring of mixotrophs will likely lead to less diverse communities due to them outcompeting strict phototrophs, and mixotrophs heavily relying on phototrophy (Urrutia-Cordero et al., 2017).

With increasing mixotrophic activity, it is possible that the efficiency of the biological carbon pump will increase due to an enhancement of transfer of biomass to larger organisms at higher trophic levels (Ward & Follows, 2016). It has been reported that larger photosynthetic cells like diatoms are being replaced in some places by autotrophic picoeukaryotes (APEs), and since these smaller cells include many known mixotrophs, this shift will likely change the transfer of carbon to the deep ocean, as smaller cells sink slower (Worden et al., 2015). The change in the composition of the microbial communities may also affect how organisms on higher trophic levels interact with their prey, as studies have shown that feeding on mixotrophs can negatively affect growth of a predator compared to feeding on strictly autotropic cells of the same species (Weithoff & Wacker, 2007).

Understanding mixotrophy is therefore important, not only to gain knowledge, but also to be able to predict future scenarios as accurately as possible. As the research of the effects of climate change is more relevant than ever, being able to create models that best represent reality is necessary, but this is not possible until the significant role of mixotrophy in marine microorganisms is understood.

1.3 Studying mixotrophic microbes

One way of studying marine mixotrophic microbes is through observing specific species in a laboratory. This has been done for several decades on many species of different phylogenetic groups (e.g. Anderson et al., 2018; Brutemark & Granéli, 2011; Caron, Porter, & Sanders, 1990; Rothhaupt, 1996; Tranvik, Porter, & Sieburth, 1989; Young & Beardall, 2003).

Another way to commonly study marine mixotrophs is to take water samples from a marine environment (e.g. Anderson, Jürgens, & Hansen, 2017; Havskum & Riemann, 1996; Pitta & Giannakourou, 2000; Unrein, Gasol, Not, Forn, & Massana, 2014). This way it is possible to analyse for example which species are present, which groups are present, which cells are

phototrophic or heterotrophic and/or which are mixotrophic, their growth rates, and cellular activities. Through studies like these, it is possible to gain an understanding of the natural environment in which these organisms exist, who they are, and how they interact with each other. Studies in natural environments, however, are difficult to perform, especially if it involves looking at mixotrophs. This is because methods of detecting mixotrophy in cells rely on living cells as they either need to be currently feeding (when using labelled prey) or the cell must be able to retain a dye. Membrane potential, and thus the ability to retain dye, is reduced significantly after cells die (Rose, Caron, Sieracki, & Poulton, 2004). Analysis must therefore be performed shortly after sample collection, which is rarely possible if the samples are collected from the ocean due to limited access to equipment and other resources. One reason that mesocosm (i.e. water enclosure) studies are useful is that they allow for a semi-natural environment while still being confined like in a laboratory experiment (**Box 3**).

Beisner, Grossart, and Gasol (2019) present an overview of available methods used to characterise phototrophic organisms that perform phagotrophy, including addition of fluorescently labelled bacteria (FLBs) to cultures to determine whether any have been ingested (e.g. Havskum & Riemann, 1996; Unrein et al., 2007), food vacuole staining in combination with microscopy, flow cytometry, and/or genome sequencing (e.g. Anderson et al., 2017; Li,

BOX 3 | Mesocosms

A mesocosm, as defined by Odum (1984), is a bounded and partially enclosed outdoor experimental setup where it is possible to study both the smaller parts like populations, and the whole ecosystem. Since Odum's definition, mesocosms have also been performed indoors (e.g. Hoppe et al., 2008; Sommer et al., 2007). Mesocosms are a middle-ground between laboratory studies (microcosms) and studying the real world (macrocosms).

Mesocosm experiments have been conducted for several decades to study microbial communities in a semi-natural environment (Odum, 1984). These studies can be conducted on land in large tanks (e.g. Lebaron et al., 1999; Urrutia-Cordero et al., 2017), or in large bags immersed in the sea or a lake (e.g. Egge & Aksnes, 1992; Lebret, Langenheder, Colinas, Östman, & Lindström, 2018). Water, that can be either unfiltered or filtered, is pumped into the enclosures, and the organisms and conditions within are followed for a length of time. In tanks, conditions can be manipulated to simulate natural conditions, and for the bags it is important to choose materials that will give conditions close to the water surrounding them. In a mesocosm experiment it is possible to get conditions close to the natural environment while still being able to keep track of the organisms and manipulate the water by for example adding nutrients.

There are some disadvantages to using mesocosm studies; mainly that there is no way to get a true control, as all enclosures are manipulated in some way, creating a bottle effect (Marrase, Lim, & Caron, 1992), though this effect is reduced with increasing volume. When having bags immersed in water, it is possible to take samples of the surrounding water, but this is not a proper control sample.

Mesocosm experiments are particularly useful to study reactions to future scenarios. However, though they can give us an idea of future reactions, it is important to keep in mind that changes in the climate happen much slower than over the few weeks or months a mesocosm experiment takes place.

Podar, & Morgan-Kiss, 2016), and use of fluorescent in situ hybridization (FISH) to label bacteria that can be quantified in food vacuoles (e.g. Gerea et al., 2012; Medina-Sánchez, Felip, & Casamayor, 2005). Genome sequencing is useful both to identify species known to be mixotrophic by sequencing deoxyribonucleic acid (DNA) (e.g. Li et al., 2016; Unrein et al., 2014), and to sequence ribonucleic acid (RNA) to examine activities (e.g. Liu, Campbell, Heidelberg, & Caron, 2016; Santoferrara, Guida, Zhang, & McManus, 2014). There are advantages and disadvantages to all methods, and the method used is usually determined by what the research is focused on.

The fluorescent dye LysoTracker Green is an example of a dye that stains acidic compartments in cells (Rose et al., 2004). This dye has been used in several studies (Anderson et al., 2018; Li et al., 2016), as well as similar dyes like LysoSensor (Carvalho & Granéli, 2006), to detect cells assumed to be mixotrophic. Though it is often assumed in studies of mixotrophy involving LysoTracker Green that it is food vacuoles and/or lysosomes that are being stained, some compartments of chloroplasts are also acidic, meaning that the dye could also accumulate there (Rose et al., 2004; Wilken et al., 2019). Carvalho and Granéli (2006) noted that in their test of a green acidotropic probe they experienced low specificity for food vacuoles, with the probe staining the cell membrane, cytoplasm, and chloroplasts. In contrast, Li et al. (2016) did not detect fluorescence from the dye in the purely photosynthetic *Chlamydomonas* species they analysed. This remains a method that needs more research to understand how LysoTracker interacts with compartments of plankton cells.

1.4 Knowledge gaps

Throughout the years most studies on mixotrophic microbes have been performed in a laboratory setting, commonly using labelled bacteria (e.g. Anderson et al., 2018; Nygaard & Tobiesen, 1993; Rothhaupt, 1996; Tranvik et al., 1989). More recently research has focused more on mixotrophy in natural or semi-natural environments (e.g. Anderson et al., 2017; Unrein et al., 2014; Unrein et al., 2007; Wilken et al., 2018), but there is still much that is unknown. Identifying mixotrophs in natural environments like the ocean is difficult, and finding methods that can be applied generally is challenging, as there is a large diversity among mixotrophic species (Stoecker et al., 2017). Even if a mixotroph is identified, there are still many unknown factors, such as which organism(s) it eats, how often it eats, the rate of photosynthesis, and what variables affects phagotrophy (Flynn et al., 2019). When studies are performed on whole communities it is not possible to know what the individual species contribute, and when

studying individual species in the laboratory it is unknown how they would behave in a natural setting and interact with other organisms.

There are many unknown factors when it comes to mixotrophy in marine microbes, and many of them are pointed out in a recent paper by Flynn et al. (2019). Since many species that were previously assumed to be strictly photo- or heterotrophic have since been discovered to be mixotrophic, the findings from earlier studies of these species may not show the whole picture. Ideally a wide range of factors (for example changing light attenuation, increased temperatures, increased availability of DOM, and other effects of climate change) should be studied to see whether they affect the mixotrophic activity or not, both in individual species and in communities, in laboratory and field experiments.

Understanding the marine food web and the interactions between the organisms it comprises, is vital to be able to predict changes, especially regarding climate change. Since the microbial loop and the microorganisms within it are the base of the entire food web, any misunderstandings here could have wide effects. This is one of the reasons why incorporating mixotrophy into mainstream marine science is so important, and why it is necessary to do more research on this topic. With the immense variety in mixotrophic microorganisms there will likely be a wide variety of reactions to the changes in their environment. Though some studies have been performed, both in the laboratory (Anderson et al., 2018; Brutemark & Granéli, 2011; Wilken et al., 2013) and in the field (Urrutia-Cordero et al., 2017; Wilken et al., 2018), to gain a better understanding of how mixotrophs react to the effects of climate change, there is still much to learn, both on the species and community level.

1.5 Objectives

The objective of this thesis was to gain a wider understanding of how mixotrophic phototrophs in a marine environment may respond to climate changes. More specifically how this group responds to the addition of brownification and dissolved iron by testing the following hypotheses:

Hypothesis 1 Brownification leads to a change in the composition of the microbial community.

Hypothesis 2 Brownification leads to a higher percentage of mixotrophic phototrophs.

Hypothesis 3 Addition of dissolved iron affects both a) the composition of the microbial community, and b) the percentage of mixotrophic phototrophs.

The hypotheses were tested by following the community in a mesocosm experiment by counting cells on a flow cytometer and using an acidotropic probe to identify potentially phagotrophic phototrophs.

2 Materials and methods

2.1 Mesocosm setup

A mesocosm experiment was conducted in June of 2019 at Espegrend Marine Biological Station (60°16'N 5°13'E), located in the Raunefjord near Bergen, Norway. June 5th was set as day 0 of the experiment, and the end was June 26th, day 21.

The 12 mesocosm bags were made of high-density polyethylene and were covered by lids made of low-density polyethylene (11m^3). Both materials are transparent to photosynthetically active radiation and ultraviolet radiation. The bags were all filled with fjord water from 6 m depth. Airlifts were placed in the bags to create circulation of the enclosed water to ensure that the water within the mesocosms was homogenous (Egge & Heimdal, 1994).

The mesocosms were each given one of four treatments of brownification (Bro) and dissolved iron (dFe): -Bro-dFe, -Bro+dFe, +Bro-dFe, or +Bro+dFe, with the minus sign meaning the substance was not added, and the plus sign meaning it was (**Fig. 3**). There were three replicates of each treatment. The mesocosms were located in the fjord attached to a floating platform, with randomised placement along the platform.

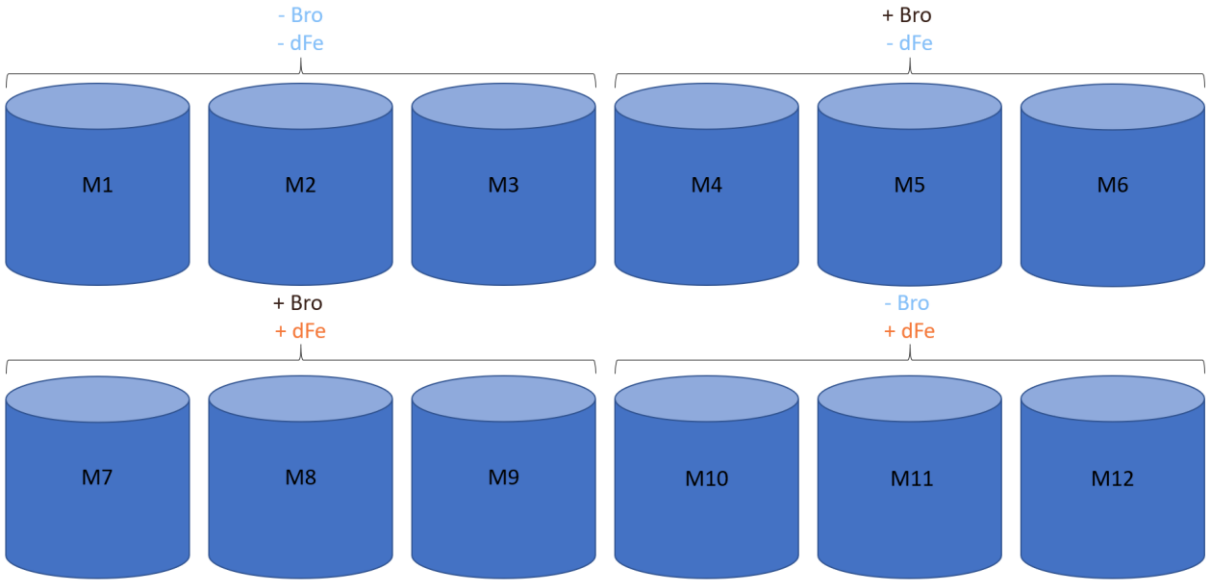

Figure 3. Illustration showing the 12 mesocosms in the experiment and which treatment they were given. M1-M3: -Bro-dFe, M4-M6: +Bro-dFe, M7-M9: +Bro+dFe, M10-M12: -Bro+dFe.

To achieve the desired level of brownification, HuminFeed® (Humintech, granulated sodium humate) was added to the +Bro mesocosms at the concentration of 2 mg L^{-1}. Dissolved iron was added to the +dFe mesocosms as the siderophore desferoxamine B (DFB) at a concentration of 70 nM. Both HuminFeed® and DFB was added at day 2 of the experiment. The nutrients

nitrate (10 µM) and phosphate (0.3 µM) were added at day 0. This was done to induce a bloom of the coccolithophore *Emiliania huxleyi*.

2.2 Flow cytometry

Samples were taken from the mesocosms at days 0, 2, 6, 8, 10, 12, 14, 16, 19, and 21. At day 0 water was pooled from all the mesocosms, while at later dates, water was collected from each mesocosm in carboys. 20 L of water were collected in the morning (between 6 and 8) at 2 m depth by gently vacuum pumping into acid-washed carboys (Segovia et al., 2017). These were then kept at 10°C. In addition, samples were collected in the same way from the fjord at days 6, 8, 10, 12, 14, 16, 19, and 21. From each carboy approximately 50 mL of water were collected (between 8 and 10). This was brought to the lab at the Department of Biological Sciences at the University of Bergen in a cooled container, and kept at 8°C.

When counting phototrophs (A. Larsen et al., 2001), samples were prepared for flow cytometry by adding 3 mL of each sample to two sets of flow cytometry tubes. One set of sample tubes was then directly counted on the flow cytometer (Attune NxT Acoustic Focusing Cytometer, Thermo Fisher Scientific; **Box 4**), while the tubes in the other had 10 µL LysoTracker® Green DND-26 (Thermo Fisher Scientific) added to them at a concentration of 3.33 µL mL^{-1}, and incubated at room temperature in the dark for 10 minutes before counting started. Settings for the flow cytometer used when counting phototrophs are given in **Appendix A1**.

For each water sample, a tube was filled with 4 mL of the sample. These samples were fixed using 20 µL mL^{-1} glutaraldehyde, and after at least 2 hours in the fridge they were flash frozen in liquid nitrogen and stored in a -80°C freezer.

To count heterotrophic nanoflagellates (HNFs) and bacteria, the frozen samples in the 4 mL tubes were thawed. This was done 5-8 months after freezing. For the bacteria counting (Marie, Partensky, Vaulot, & Brussaard, 1999), a dilution series of 5x, 10x, 50x, 100x, 500x, and 1,000x was prepared for each sample. The samples were vortexed before being diluted in filtered (0.2 µm, Whatman) TE-buffer to a total volume of 1 mL. 10 µL SYBR Green (Thermo Fisher Scientific) was then added to the tubes before mixing by vortexing. The samples were then incubated at room temperature in the dark for at least 10 minutes. For counting of HNFs (Zubkov, Burkill, & Topping, 2007), 3 mL vortexed sample was added to flow cytometry tubes before the addition of 30 µL SYBR green, to a final concentration of 10 µL mL^{-1}. The samples were vortexed and incubated at room temperature in the dark for approximately 2 hours. When counting both HNFs and bacteria, the tubes were vortexed shortly before counting on the flow

cytometer (Attune NxT Acoustic Focusing Cytometer, Thermo Fisher Scientific). Settings for the flow cytometer used when counting both bacteria and HNFs are given in **Appendix A1**.

BOX 4 | How flow cytometry works

Flow cytometry is a technique that is used to count cells in a liquid medium and examine their properties (Madigan, Bender, Buckley, Sattley, & Stahl, 2019). The technique was first developed for biomedical use, but has been used in marine studies since the late 1970s, frequently in studies of marine microbes to enumerate and characterise them (Munn, 2011; Sosik, Olson, & Armbrust, 2010).

A modern flow cytometer has three main components: the fluidics system, the optical system, and the electronics (Marie, Simon, & Vaulot, 2005). The fluidics system organises a sample that has been taken up into a single-file stream of cells. The cells in the sample are transported to the point where a laser light meets the stream of cells, and when the beam of laser light meets a cell or another particle, the light will scatter and fluoresce (**Fig. 4**) (Marie et al., 2005; Sosik et al., 2010). This is the optical system. The scattering of light is measured by the electronics as forward angle scatter (FSC) and side angle scatter (SSC), which are correlated to cell size, and there are also detectors that measure the fluorescence emitted by fluorophores associated with the cell (Marie et al., 2005). All the information gathered on each cell can be viewed and analysed in the computer software, where it is possible to get figures like dot plots, histograms, and density plots, with the desired properties as variables.

Phototrophic cells naturally have fluorescence due to their photosynthetic pigments, of which chlorophyll a, phycoerythrin, and phycocyanin are most common, which allows for identification of such cells even untreated (Marie et al., 2005; Sosik et al., 2010). Both chlorophyll a and phycoerythrin are excited by a 488 nm laser, which is commonly used, making them ideal properties to analyse (Marie et al., 2005). Based on their properties, such as size and pigmentation, it is possible to differentiate between groups or even species of phototrophs (Olson, Zettler, & Anderson, 1989; Sosik et al., 2010). For example, coccolithophores covered in coccoliths (cell coverings of calcium carbonate) can be identified due to their depolarisation of forward scattered light (Olson et al., 1989), the cyanobacteria *Synechococcus* can be identified due to its high level of phycoerythrin (Olson, Chisholm, Zettler, & Armbrust, 1990), and picoeukaryotes can be identified based on size (Sosik et al., 2010).

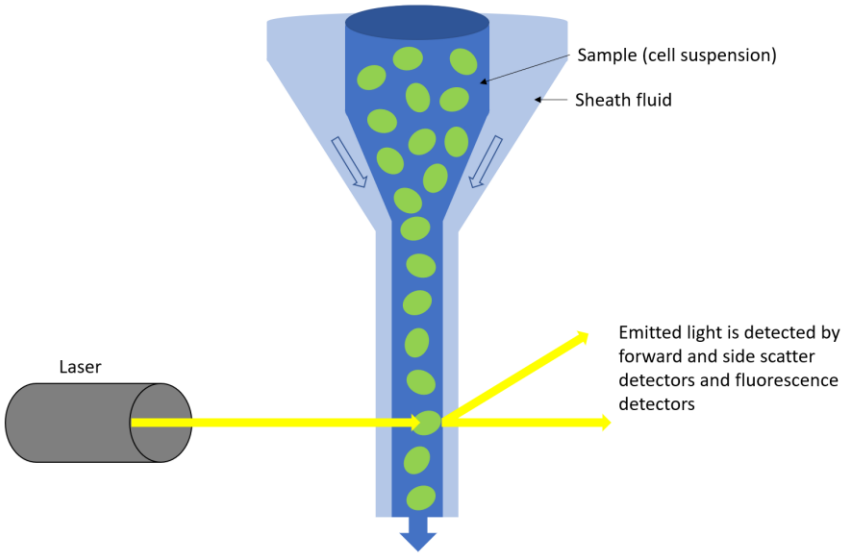

Figure 4. Illustration showing how a flow cytometer works. Arrows indicate direction of fluid/light. The sample (most often a cell suspension) is narrowed to a stream of single-cell width with help of the sheath fluid. Each cell then goes through a beam of laser light, which scatters the light and the light is detected by different detectors: forward scatter, side scatter, and different fluorescence detectors (normally able to detect red, yellow, and/or green light).

During flow cytometry, HNFs were discriminated from autotrophic nanoeukaryotes (ANEs) based on green (SYBR Green) vs red (chlorophyll) fluorescence and bacteria based on green fluorescence (**Figs. 5c** and **5d**) (Zubkov et al., 2007). Autotrophic picoeukaryotes (APEs), ANEs, and *Synechococcus* sp. were discriminated based on red vs orange (phycoerythrin) fluorescence (**Fig. 5b**) (Bratbak et al., 2011; A. Larsen et al., 2004). *E. huxleyi* was identified in plots of side scatter vs red fluorescence due to elevated side scatter caused by their coccoliths (**Fig. 5a**) (Jacquet et al., 2002). Cryptophytes were identified due to their high orange fluorescence (**Fig. 5b**) (Bratbak et al., 2011).

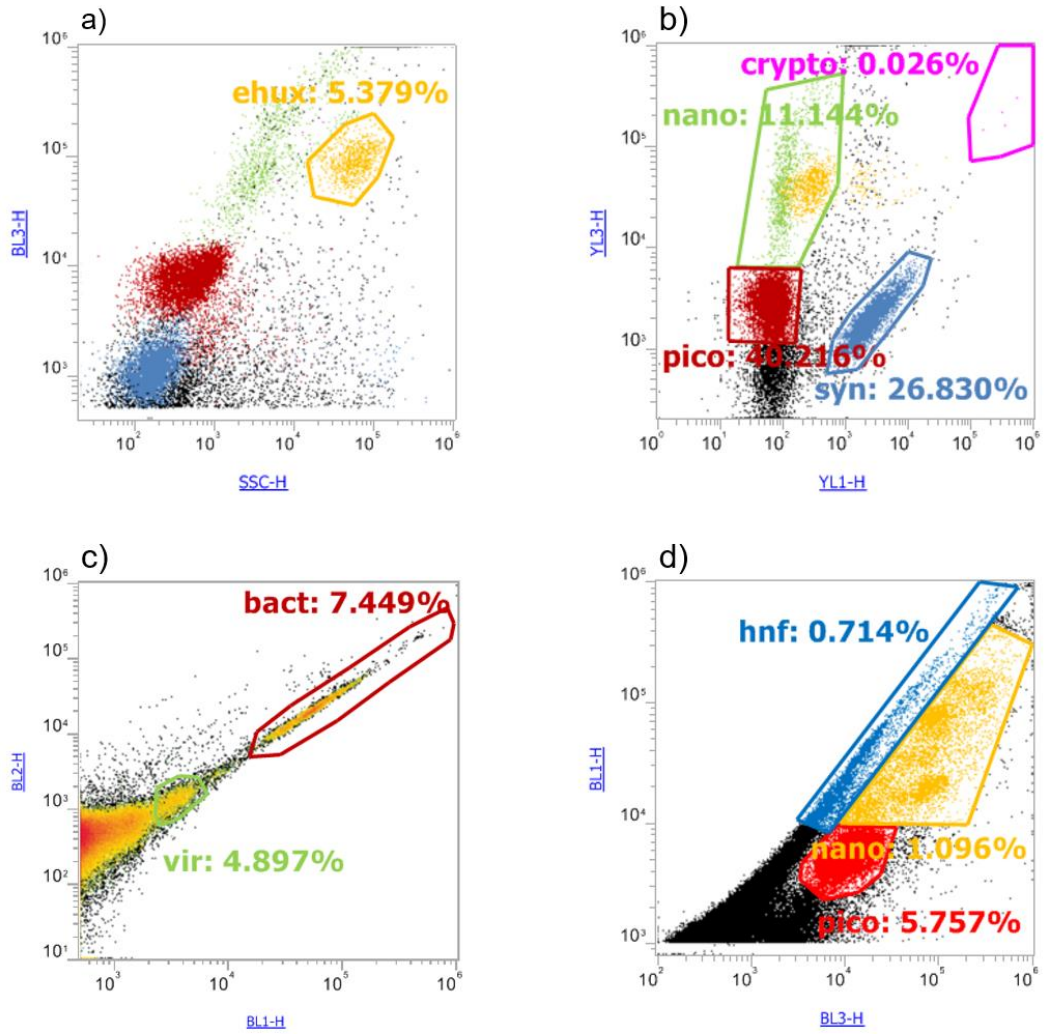

Fig. 5. Plots from the Attune software showing how the different groups were discriminated. Percentages show what percentage of total events occurred inside the gate. a) dot plot showing how side scatter (SSC) vs red fluorescence (BL3) plot was used to identify the coccolithophore *Emiliania huxleyi* ("ehux"), b) dot plot showing how orange (YL1) vs red (YL3) fluorescence was used to identify autotrophic nanoeukaryotes (ANEs, "nano"), cryptophytes ("crypto"), autotrophic picoeukaryotes (APEs, "pico"), and *Synechococcus* sp. ("syn"), c) density plot showing how green (BL1) vs orange (BL2) fluorescence was used to identify bacteria ("bact") and a group of possible viruses not discussed in this thesis ("vir"), d) dot plot showing how red (BL3) vs green (BL1) fluorescence was used to discriminate heterotrophic nanoflagellates (HNFs, "hnf") from ANEs ("nano") and APEs ("pico").

2.3 Data analysis

The Attune software was used to calculate the percentage of possibly mixotrophic cells. For each sample an overlay of the BL1 (green fluorescence) histograms with and without LysoTracker was made for each organism group. A threshold marker was placed on the histogram without LysoTracker in such a way that <2% of the counted cells were above it (**Fig. 6**). The cells on the sample with LysoTracker that were above this threshold were considered to be possible mixotrophs and were called "LysoTracker positive cells".

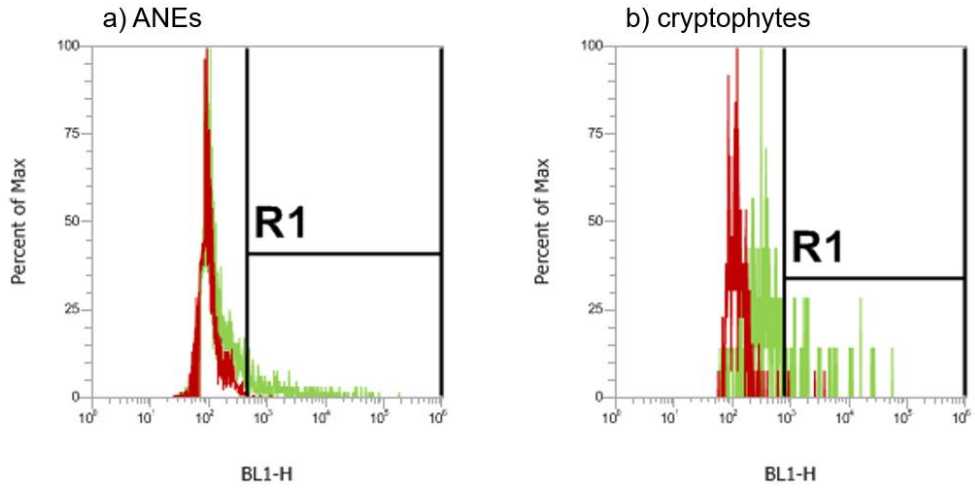

Fig. 6. Examples of histogram overlays showing samples with (light green colour) and without (dark red colour) LysoTracker added. Cells represented inside the R1 gate were considered LysoTracker positive. a) histogram of counted autotrophic nanoeukaryote (ANE) cells where 0.15% of the non-stained and 13% of the stained samples were inside the R1 gate, b) histogram of counted cryptophyte cells where 1.0% of the non-stained and 22% of the stained samples were inside the R1 gate.

2.4 Statistical analysis

Statistical analyses were performed in R version 3.6.0 (The R Foundation). For each organism group on each sample day the two treatments (-Bro and +Bro, or -dFe and +dFe) were compared, using a two-way mixed ANOVA with the treatment as the between-subjects factor and sample day as the within-subjects factor (Kassambara, n.d.). An α-value of 0.05 was used, as well as adjusted p-values that correct for type I error (i.e. rejection of a null hypothesis without a true effect) were used to determine statistical significance.

3 Results

Where no SE is given only one sample was collected. Sampling of the fjord started at day 6.

3.1 Abundances of microbial groups

3.1.1 Autotrophic nanoeukaryotes

For the -Bro treatment (no HuminFeed® added), the mean abundance of autotrophic nanoeukaryotes (ANEs) spanned from $8.20\times10^{2} \pm 6.60\times10^{1}$ cells mL^{-1} to $4.40\times10^{3} \pm 7.41\times10^{2}$ cells mL^{-1} (**Fig. 7**). The initial abundance was 1.50×10^{3} cells mL^{-1} for both the -Bro and +Bro treatment (with HuminFeed® added). In -Bro mesocosms two peaks, one at day 6 at $2.64\times10^{3} \pm 1.59\times10^{2}$ cells mL^{-1}, and one at day 19 at $4.40\times10^{3} \pm 7.41\times10^{2}$ cells mL^{-1}, were observed. Abundances in +Bro treated mesocosms ranged from $6.89\times10^{2} \pm 8.21\times10^{1}$ cells mL^{-1} to $2.97\times10^{3} \pm 1.55\times10^{2}$ cells mL^{-1} with a peak at day 6 at $2.97\times10^{3} \pm 1.55\times10^{2}$ cells mL^{-1} mean abundances below 1.50×10^{3} cells mL^{-1} after day 10. Abundance in the fjord ranged from 7.13×10^{2} cells mL^{-1} to 4.92×10^{3} cells mL^{-1}, with a peak at day 10 at 4.17×10^{3} cells mL^{-1}, and a rapid increase from day 16 to the end of the experiment at day 21, with an abundance of 4.92×10^{3} cells mL^{-1}.

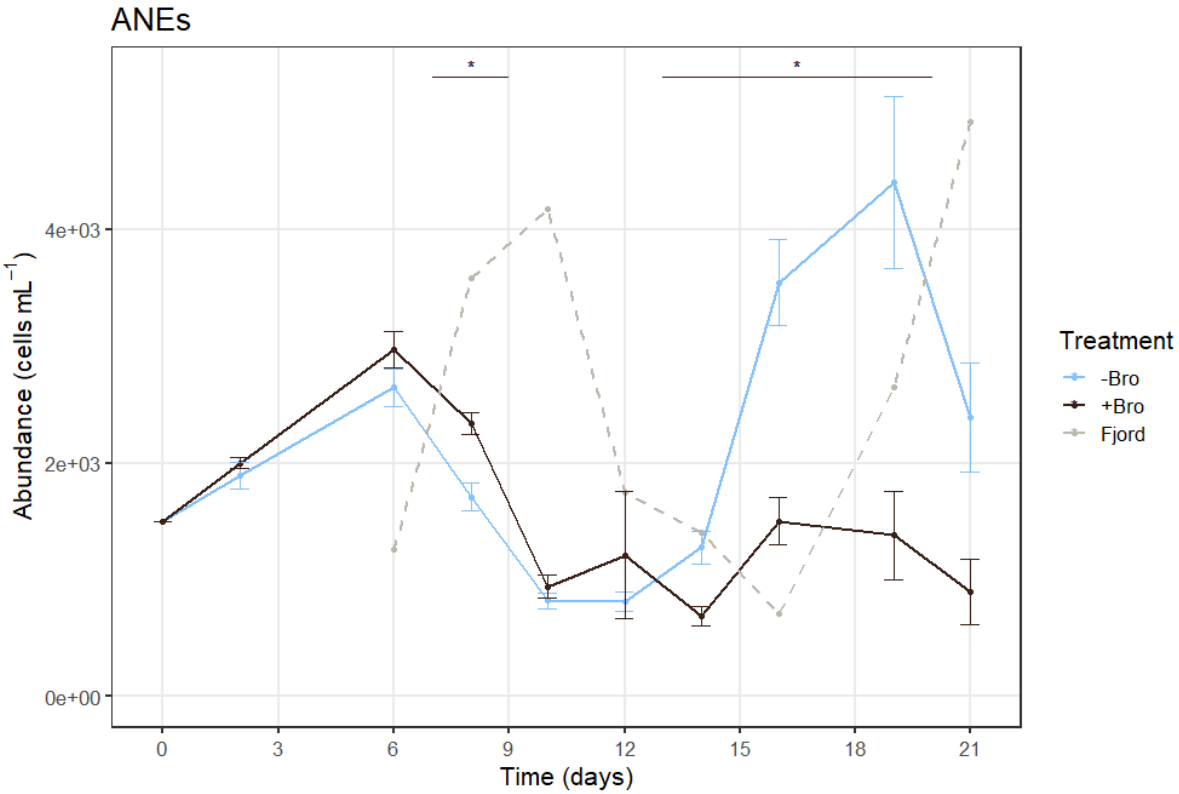

Figure 7. Abundance (cells mL^{-1}) of autotrophic nanoeukaryotes (ANEs) on each sample day of the experiment. The dashed grey line shows the abundance in the fjord, while the brown and blue lines show the mean ± SE with and without brownification, respectively. n=6 for both the -Bro and +Bro treatments (days 2-21), n=1 for the fjord, n=1 for day 0. Stars indicate a significant difference between the -Bro and the +Bro treated mesocosms.

3.1.2 Cryptophytes and *Emiliania huxleyi*

The initial abundance of cryptophytes in both -Bro and +Bro treated mesocosms was 1.22×10^{2} cells mL^{-1} (**Fig. 8a**). The mean abundance peaked at day 2 in both treatments, at $1.45\times10^{2} \pm 1.85\times10^{1}$ cells mL^{-1} in the -Bro mesocosms and $1.66\times10^{2} \pm 1.09\times10^{1}$ cells mL^{-1} in the +Bro mesocosms. Abundances in the -Bro mesocosms ranged from $3.67\times10^{0} \pm 0.843\times10^{0}$ cells mL^{-1} to $1.45\times10^{2} \pm 1.85\times10^{1}$ cells mL^{-1}, and in the +Bro mesocosms from $1.00\times10^{1} \pm 1.95\times10^{0}$ cells mL^{-1} to $1.66\times10^{2} \pm 1.09\times10^{1}$ cells mL^{-1}. Both treatments had mean abundances at $<5.00\times10^{1}$ cells mL^{-1} from day 6 (-Bro treatment) or day 8 (+Bro treatment). Abundance in the fjord ranged from 5.30×10^{1} cells mL^{-1} to 3.09×10^{2} cells mL^{-1} and peaked at day 10 (3.09×10^{2} cells mL^{-1}) and day 14 (2.75×10^{2} cells mL^{-1}). From day 19 (5.30×10^{1} cells mL^{-1}) there was a rapid increase until the end of the experiment (day 21) at 2.23×10^{2} cells mL^{-1}.

Initial abundance of *E. huxleyi* in both -Bro and +Bro treated mesocosms was 5.09×10^{2} cells mL^{-1} (**Fig. 8b**). Abundance in the -Bro mesocosms spanned from $1.25\times10^{2} \pm 4.16\times10^{1}$ cells mL^{-1} to 5.09×10^{2} cells mL^{-1}. There was a decrease until day 6 (2.68×10^{2} cells mL^{-1}), before a peak at day 8 at $3.86\times10^{2} \pm 3.54\times10^{1}$ cells mL^{-1}. From day 14 (1.25×10^{2} cells mL^{-1}) there was an increase in abundance until the end of the experiment (day 21) at $3.78\times10^{2} \pm 2.61\times10^{2}$ cells mL^{-1}, with large standard errors at days 16, 19, and 21. Abundance in the +Bro mesocosms ranged from $7.75\times10^{1} \pm 1.51\times10^{1}$ cells mL^{-1} to $5.24\times10^{2} \pm 6.15\times10^{1}$ cells mL^{-1}, decreased until day 2 (3.17×10^{2} cells mL^{-1}), and then peaked at $5.24\times10^{2} \pm 6.15\times10^{1}$ cells mL^{-1} at day 8. It decreased rapidly until day 14 ($7.75\times10^{1} \pm 1.51\times10^{1}$ cells mL^{-1}) and stayed below 2.00×10^{2} cells mL^{-1} until the end of the experiment (day 21). Abundance in the fjord decreased from day 6 (6.30×10^{2} cells mL^{-1}) to day 19 (5.20×10^{1} cells mL^{-1}), before increasing to 7.30×10^{1} cells mL^{-1} at the end of the experiment (day 21).

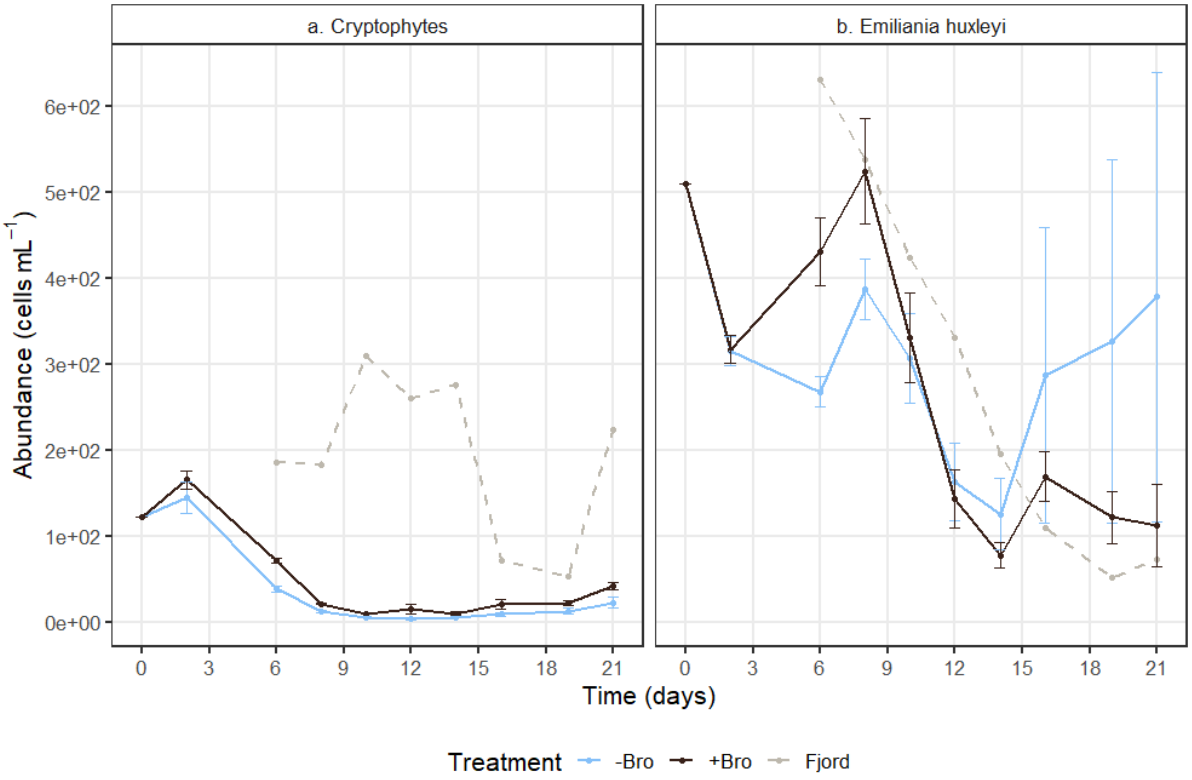

Figure 8. Abundance (cells mL^{-1}) of cryptophytes (a) and the coccolithophore *Emiliania huxleyi* (b) on each sample day of the experiment. The dashed grey line shows the abundance in the fjord, while the brown and blue lines show the mean ± SE with and without brownification, respectively. n=6 for both the -Bro and +Bro treatments (days 2-21), n=1 for the fjord, n=1 for day 0.

3.1.3 Autotrophic picoeukaryotes

For both -Bro and +Bro treatments initial autotrophic picoeukaryote (APE) abundance was 4.08×10^3 cells mL^{-1} (**Fig. 9a**). In -Bro mesocosms the abundance spanned from $1.75\times10^3 \pm 7.06\times10^2$ cells mL^{-1} to $2.78\times10^4 \pm 3.33\times10^3$ cells mL^{-1}, with a peak at day 6 at $2.78\times10^4 \pm 3.33\times10^3$ cells mL^{-1}. In the +Bro mesocosms APE abundance peaked at day 8 with a mean abundance of $6.72\times10^4 \pm 1.85\times10^3$ cells mL^{-1} and spanned from $1.73\times10^3 \pm 4.92\times10^2$ cells mL^{-1} to $6.72\times10^4 \pm 1.85\times10^3$ cells mL^{-1}. In both treatments mean abundances were $<8.00\times10^3$ cells mL^{-1} after day 10. In the fjord abundances remained below 1.50×10^4 cells mL^{-1} throughout the experiment, with the highest values being at day 10 at 1.34×10^4 cells mL^{-1}, and the lowest abundance being at day 16 at 6.22×10^2 cells mL^{-1}. APE abundance increased towards the end of the experiment, reaching an abundance of 9.45×10^3 cells mL^{-1} at day 21.

The initial abundance of *Synechococcus* sp. for both the -Bro and +Bro treatments was 9.54×10^3 cells mL^{-1} (**Fig. 9b**). For the -Bro treatment, the abundance spanned from $1.52\times10^3 \pm 5.11\times10^2$ cells mL^{-1} to $1.99\times10^4 \pm 1.77\times10^1$ cells mL^{-1}. From day 2 *Synechococcus* sp. abundance decreased until day 12 ($1.52\times10^3 \pm 5.11\times10^2$ cells mL^{-1}), before an exponential increase lasting

until the end of the experiment (day 21), reaching $1.99\times10^4 \pm 1.77\times10^1$ cells mL^{-1}, took place. Abundances in +Bro mesocosms ranged from $4.40\times10^3 \pm 5.53\times10^2$ cells mL^{-1} to $2.95\times10^4 \pm 3.53\times10^3$ cells mL^{-1}, and peaked at day 8 at $1.56\times10^4 \pm 4.70\times10^2$ cells mL^{-1} before decreasing to $4.40\times10^3 \pm 5.53\times10^2$ cells mL^{-1} at day 14. From day 14 a rapid increase until day 21 to $2.95\times10^4 \pm 3.53\times10^3$ cells mL^{-1} was observed. The fjord abundance ranged from 1.00×10^4 cells mL^{-1} to 4.47×10^4 cells mL^{-1}, with a peak at day 10 at 4.47×10^4 cells mL^{-1}. From 1.00×10^4 cells mL^{-1} at day 16, an increase until day 21 to 2.93×10^4 cells mL^{-1} was observed.

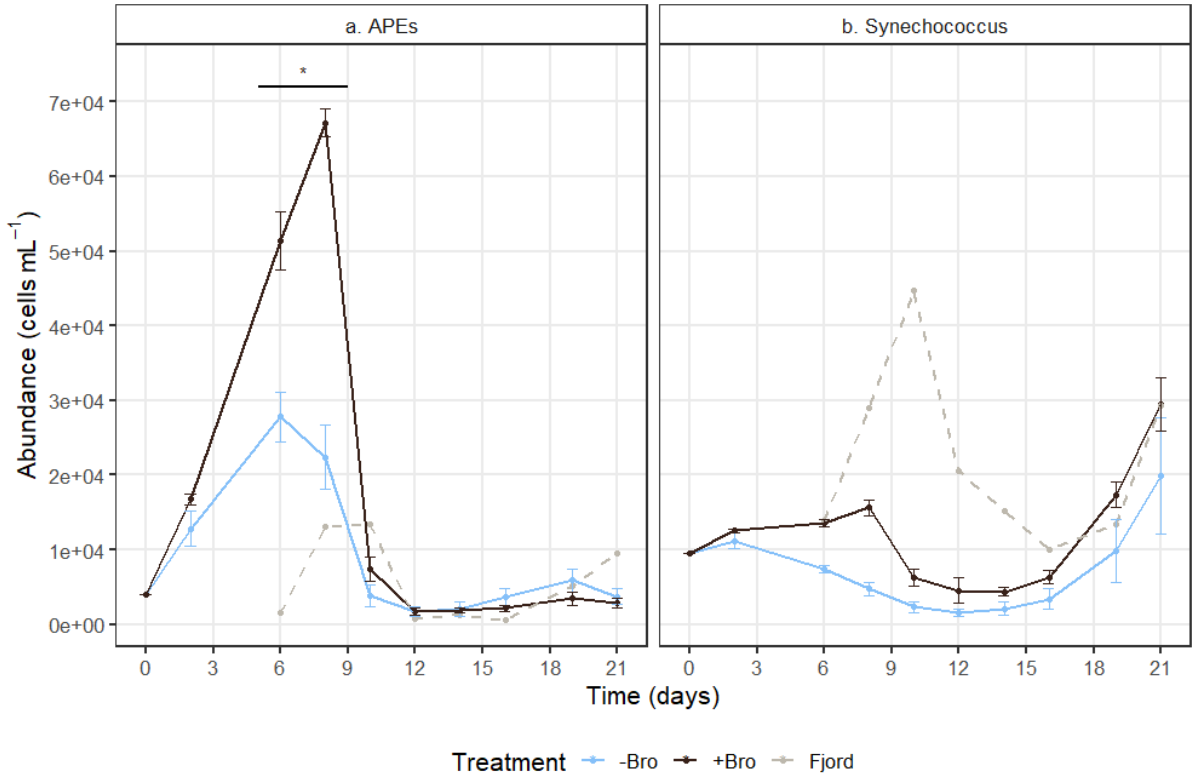

Figure 9. Abundance (cells mL^{-1}) of autotrophic picoeukaryotes (APEs) (a) and the cyanobacterium *Synechococcus* sp. (b) on each sample day of the experiment. The dashed grey line shows the abundance in the fjord, while the brown and blue lines show the mean ± SE with and without brownification, respectively. n=6 for both the -Bro and +Bro treatments (days 2-21), n=1 for the fjord, n=1 for day 0. Star indicates a significant difference between the -Bro and the +Bro treated mesocosms.

3.1.3 Bacteria

The bacterial abundance at day 0 in both the -Bro and the +Bro mesocosms was 8.88×10^5 cells mL^{-1} (**Fig. 10**). Abundance in the -Bro mesocosms ranged from $4.19\times10^5 \pm 6.71\times10^4$ cells mL^{-1} to $1.19\times10^6 \pm 2.31\times10^4$ cells mL^{-1}, and peaked at day 2 ($1.19\times10^6 \pm 2.31\times10^4$ cells mL^{-1}) and day 14 ($5.96\times10^5 \pm 5.50\times10^4$ cells mL^{-1}). From day 16 the abundance increased until the end of the experiment (day 21) to $8.78\times10^5 \pm 5.82\times10^4$ cells mL^{-1}. Abundance in the +Bro mesocosms spanned from $4.62\times10^5 \pm 4.93\times10^4$ cells mL^{-1} to $1.17\times10^6 \pm 3.04\times10^4$ cells mL^{-1}. It peaked at $1.17\times10^6 \pm 3.04\times10^4$ cells mL^{-1} at day 2 and day 6, decreased until day 16 (4.62×10^5

cells mL^{-1}), and peaked again at day 19 at $6.61\times10^5 \pm 8.45\times10^4$ cells mL^{-1}. Abundances in the fjord spanned from 3.99×10^5 cells mL^{-1} to 9.73×10^5 cells mL^{-1}, starting at 9.73×10^5 cells mL^{-1} at day 6, then decreasing until day 8 at 7.05×10^5 cells mL^{-1}. It peaked at day 12 at 9.45×10^5 cells mL^{-1} before it decreased until day 19 (3.99×10^5 cells mL^{-1}) and then increased until the end of the experiment (day 21) to 4.98×10^5 cells mL^{-1}.

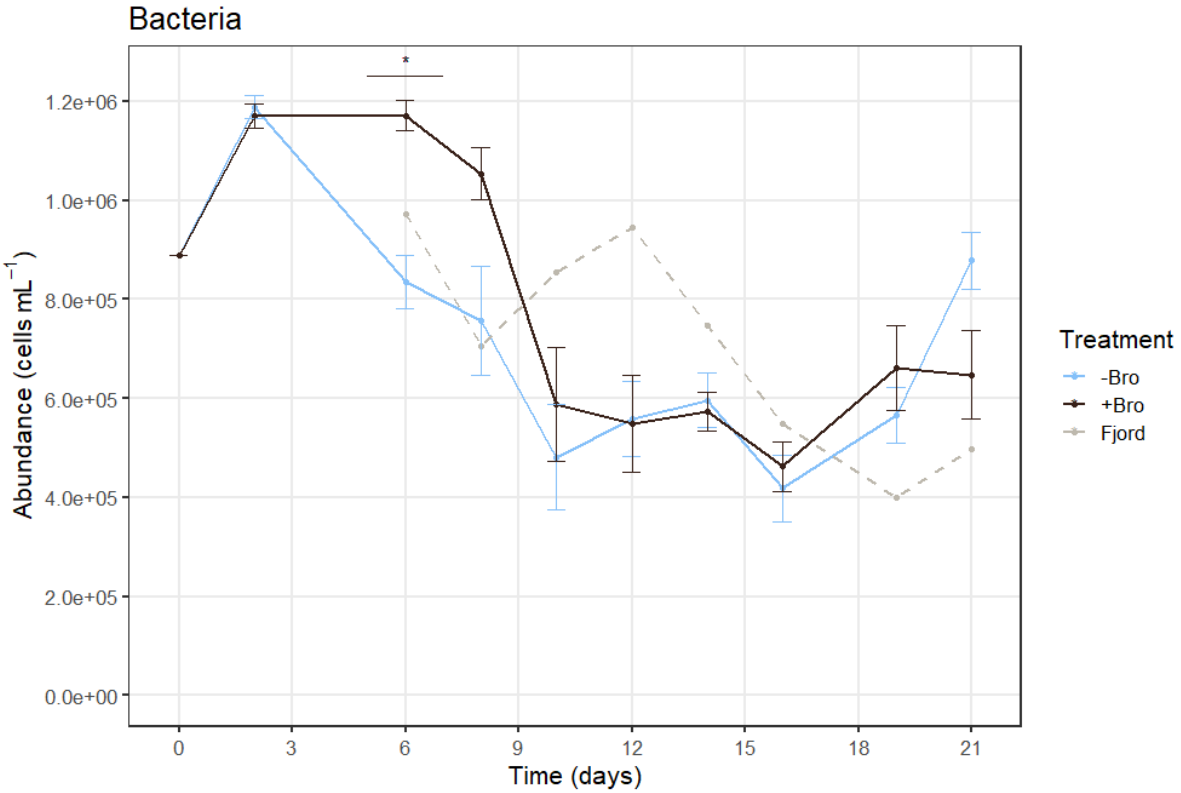

Figure 10. Abundance in cells mL^{-1} of bacteria on each sample day of the experiment. The dashed grey line shows the abundance in the fjord, while the brown and blue lines show the mean ± SE with and without brownification, respectively. n=6 for both the -Bro and +Bro treatments (days 2-21), n=1 for the fjord, n=1 for day 0. Star indicates a significant difference between the -Bro and the +Bro treated mesocosms.

3.1.4 Heterotrophic nanoflagellates

The initial abundance of heterotrophic nanoflagellates (HNFs) in both the -Bro and +Bro treated mesocosms was 1.02×10^3 cells mL^{-1} (**Fig. 11**). Abundance in the -Bro mesocosms spanned from $7.00\times10^2 \pm 6.19\times10^1$ cells mL^{-1} to $3.36\times10^3 \pm 1.51\times10^2$ cells mL^{-1}, peaked at day 6 ($1.47\times10^3 \pm 8.30\times10^1$ cells mL^{-1}), decreased until day 10 (7.00×10^2 cells mL^{-1}), and peaked again at day 16 ($3.36\times10^3 \pm 1.51\times10^2$ cells mL^{-1}). Abundance in the +Bro mesocosms spanned from $9.93\times10^2 \pm 1.24\times10^2$ cells mL^{-1} to $2.46\times10^3 \pm 6.79\times10^1$ cells mL^{-1}. It peaked at day 6 ($2.46\times10^3 \pm 6.79\times10^1$ cells mL^{-1}) and day 16 ($2.29\times10^3 \pm 2.76\times10^2$ cells mL^{-1}) and reached approximately 1.00×10^3 cells mL^{-1} both before, between, and after the peaks. Abundance in the fjord spanned from 3.93×10^2 cells mL^{-1} to 2.26×10^3 cells mL^{-1}. It started at 1.15×10^3 cells

mL^{-1} at day 6 (1.15×10^3 cells mL^{-1}) and had a peak at day 12 (2.26×10^3 cells mL^{-1}), then decreased until day 16 (3.93×10^2 cells mL^{-1}) and increased to 6.71×10^2 cells mL^{-1} at the end of the experiment (day 21). An extreme outlier at day 12 (M6) with an HNF abundance of 8.59 × 10^3 cells mL^{-1} was excluded as this was considered a measuring error.

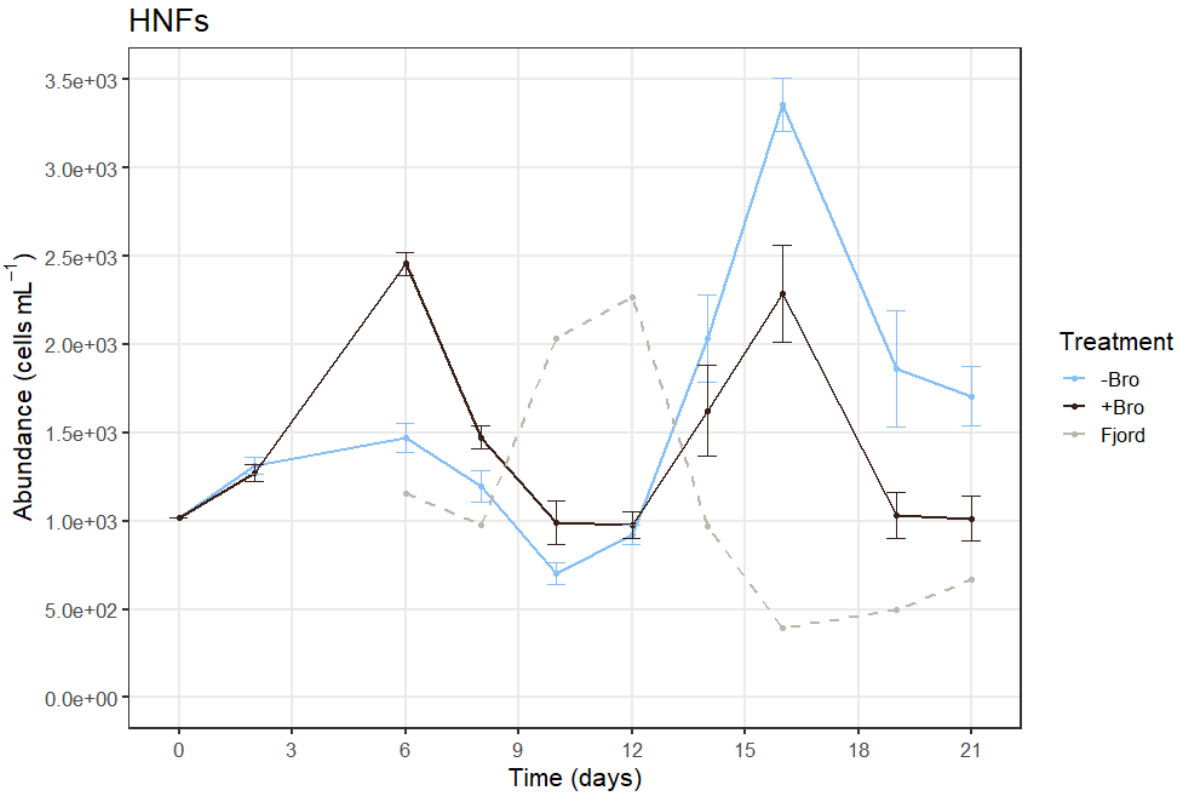

Figure 11. Abundance in cells mL^{-1} of heterotrophic nanoflagellates (HNFs) on each sample day of the experiment. The dashed grey line shows the abundance in the fjord, while the brown and blue lines show the mean ± SE with and without brownification, respectively. n=6 for both the -Bro and +Bro treatments (days 2-21), n=1 for the fjord, n=1 for day 0.

3.2 Percentages of LysoTracker positive cells

3.2.1 Autotrophic nanoeukaryotes

The initial percentage of LysoTracker positive autotrophic nanoeukaryote (ANE) cells was 56% for both the +Bro and the -Bro treated mesocosms (**Fig. 12a**). The mean percentages of LysoTracker positive cells in the -Bro mesocosms ranged from 20% ± 3.8% to 59% ± 3.6%. It decreased to 27% ± 6.8% at day 2, and from day 12 (20% ± 3.8%) it increased until a peak at day 19 at 59% ± 3.6%. Mean percentages in the +Bro mesocosms ranged from 13% ± 1.5% to 56%, decreased to 28% ± 1.3% at day 2, and continued to decrease until day 10 (13% ± 1.5%). In +Bro mesocosms the mean percentage peaked at day 19 at 45% ± 4.6%. Percentages in the fjord ranged from 6.3% to 61%, and peaked at days 8 (25%), 12 (18%), and 19 (61%). At day 14, an outlier not included in the line graph due to an error in the method, the mean percentage

of LysoTracker positive cells in -Bro mesocosms was 68% ± 2.5% and 63% ± 2.7% in +Bro mesocosms, and the percentage in the fjord was 18%.

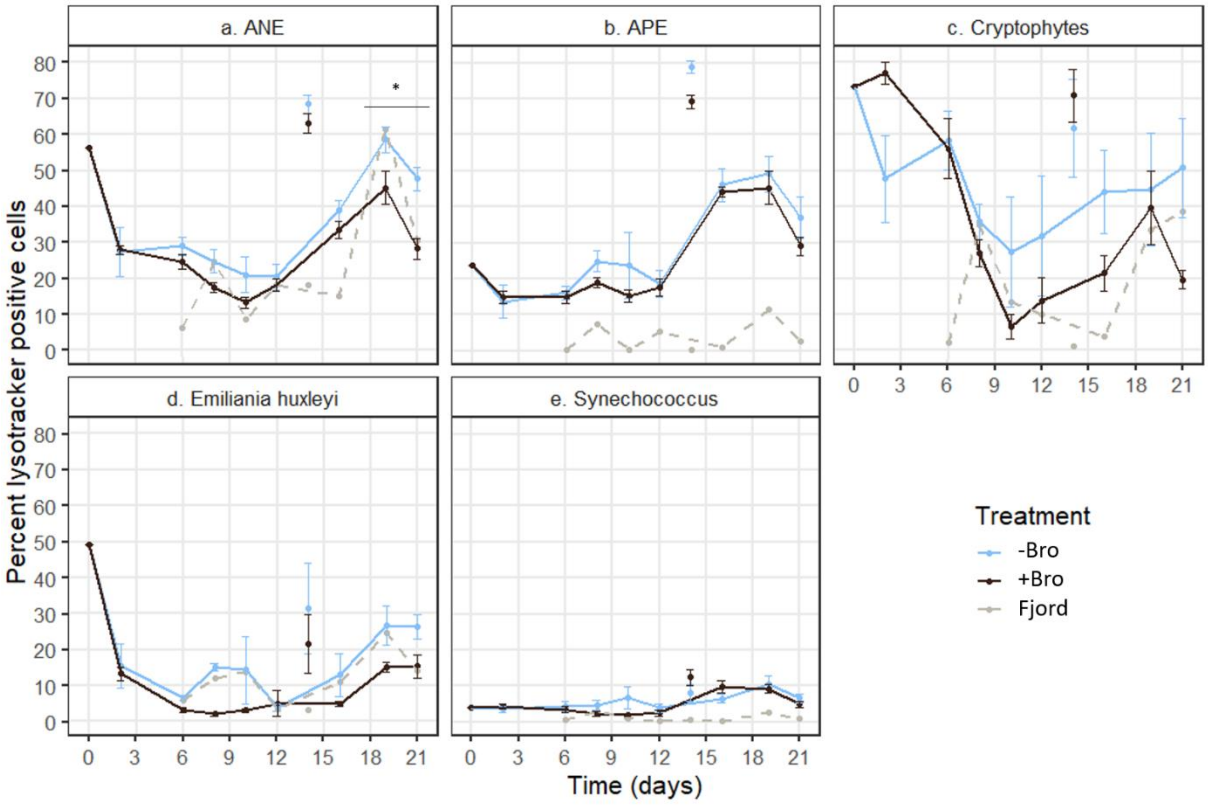

Figure 12. Percentages of LysoTracker positive cells on each sample day of the experiment for each group; autotrophic nanoeukaryotes (ANEs) (a), autotrophic picoeukaryotes (APEs) (b), cryptophytes (c), *Emiliania huxleyi* (d), and *Synechococcus* sp. (e). The grey lines show the fjord percentage, while the brown and blue lines show the mean percentage ± SE with and without brownification, respectively. The points on day 14 show the mean percentage ± SE when an error was made when preparing the samples. n=6 for both the -Bro and +Bro treatments (days 2-21), n=1 for the fjord, n=1 for day 0. The star indicates a significant difference between the -Bro and the +Bro treated mesocosms.

3.2.2 Cryptophytes and *Emiliania huxleyi*

The initial percentage of LysoTracker positive cryptophyte cells in both -Bro and the +Bro treated mesocosms was 73% (**Fig. 12c**). Mean percentages in the -Bro mesocosms ranged from 27% ± 15% to 73%, and decreased until day 2 to 48% ± 12%. A peak was observed at day 6 (58% ± 8.3), then the percentage decreased until day 10 (27% ± 15%) before increasing until the end of the experiment (day 21) to 51% ± 14%. The mean percentages of LysoTracker positive cryptophytes in +Bro mesocosms ranged from 6.5% ± 3.3% to 77% ± 3.1% and peaked at day 2 (77% ± 3.1%) and day 19 (40% ± 10%). At day 10, between the two peaks, the mean percentage was 6.5% ± 3.3%. The percentage in the fjord of LysoTracker positive cells ranged from 1.2% to 38%, had a peak at day 8 at 35%, decreased until day 16 (3.9%), and increased until day 21 to 38%. At day 14, an outlier not included in the line graph due to an error in the

method, the mean percentage in the -Bro mesocosms was 62% ± 14% and in the +Bro treatment 71% ± 7.4%, and the percentage in the fjord was 1.2%.

The mean percentages of LysoTracker positive cells of *E. huxleyi* ranged from 3.9% ± 1.1% to 49% in the -Bro mesocosms, and from 2.1% ± 0.44% to 49% in the +Bro mesocosms (**Fig. 12d**). The initial percentage in both treatments was 49%. The mean percentage in the -Bro mesocosms decreased until day 6 to 6.6% ± 0.56% and peaked at day 8 at 15% ± 1.0%. From day 12 (3.9%) it increased to a second peak at day 19 (27% ± 5.6%). The percentage in the +Bro mesocosms decreased until day 8 (2.1% ± 0.44%), increased until day 12 to 5.1% ± 3.5%, and increased from day 16 (4.9% ± 0.70%) until day 21 to 15% ± 3.3%. The percentages in the fjord ranged from 3.4% to 25% and peaked at day 10 (14%) and day 19 (25%). At day 14, an outlier not included in the line graph due to an error in the method, the mean percentage of LysoTracker positive cells in -Bro mesocosms was 31% ± 13% and 22% ± 8.2% in +Bro mesocosms, and the percentage in the fjord was 3.3%.

3.2.3 Autotrophic picoeukaryotes

The initial percentage of LysoTracker positive autotrophic picoeukaryote (APE) cells was 24% for both the -Bro and the +Bro treated mesocosms (**Fig. 12b**). Mean percentages in the -Bro mesocosms ranged from 14% ± 4.7% to 49% ± 4.8%. It decreased until day 2 (14% ± 4.7%), then peaked at 25% ± 3.0% at day 8. From day 8 it decreased until day 12 (19% ± 3.7%), then increased to another peak at day 19 (49% ± 4.8%). The percentages in the +Bro mesocosms ranged from 15% ± 1.8% to 45% ± 4.6%, decreased until day 2 (15% ± 1.8%), and remained <20% until day 14. It peaked at day 19 at 45% ± 4.6%. The percentage of LysoTracker positive cells in the fjord samples remained <10% throughout the experiment, except for a peak at day 19 (12%). At day 14, an outlier not included in the line graph due to an error in the method, the mean percentage in -Bro mesocosms was 79% ± 1.7% and 69% ± 1.9% in +Bro mesocosms, and the percentage in the fjord was 0.41%.

The initial percentage of LysoTracker positive *Synechococcus* sp. cells was 3.9% in both -Bro and +Bro treated mesocosms (**Fig. 12e**). The mean percentages in -Bro mesocosms ranged from 3.5% ± 0.88% to 10% ± 2.5%, and peaked at day 10 at 6.8% ± 3.1%. From day 12 (3.9% ± 1.2%) it increased to another peak at day 19 (10% ± 2.5%). The mean percentages in the +Bro mesocosms ranged from 2.1% ± 0.33% to 9.7% ± 1.7%. From day 2 (4.4% ± 0.73%) it decreased until day 10 (2.1% ± 0.33%), then peaked at day 16 at 9.7% ± 1.7%. The percentages of LysoTracker positive cells in the fjord ranged from 0.18% to 2.9%, and peaked at day 8

(2.9%) and day 19 (2.6%). At day 14, an outlier not included in the line graph due to an error in the method, the mean percentage was 8.1% ± 2.5% in -Bro mesocosms and 12% ± 2.2% in +Bro mesocosms, and the percentage in the fjord was 0.55%.

4 Discussion

4.1 Effects of brownification on the composition of the community

4.1.1 Succession patterns of the different groups

Generally, abundances initially increased to a peak on days 2-8, then decreased before either staying low or again increasing during the second half of the experiment (**Figs. 7-11**). This mostly compares well with other experiments at the same location (Paulino, Egge, & Larsen, 2008; Segovia et al., 2017). In addition to the groups accounted for in this study, larger grazers such as ciliates likely affected abundances by grazing on both nano- and pico-sized organisms (Rassoulzadegan, Laval-Peuto, & Sheldon, 1988), and viruses are always present and play an important role for protist communities (Suttle, 2005). However, none of these groups were targets for the main objectives of the current study.

Autotrophic nanoeukaryotes (ANEs), which peaked twice in some mesocosms and were found in high abundances in the fjord (**Fig. 7**), normally bloom during early summer in temperate areas (Andersson, Haecky, & Hagström, 1994; Tarran & Bruun, 2015), during which this experiment took place. The mesocosms were filled with water with relatively high abundances of *Emiliania huxleyi* (**Fig. 8b**). *E. huxleyi* typically blooms on the west coast of Norway during this time of year (e.g. Tyrrell & Merico, 2004, and references therein), and its rapid decrease in abundance in the fjord outside the enclosures indicates a demising bloom when the filling took place.

Cryptophytes may bloom both in spring and late summer in the Raunefjord depending on the year (Paulino et al., 2018), and in late summer/early autumn in other temperate areas (Tarran & Bruun, 2015). Therefore, not unexpectedly, initial cryptophyte abundances were low in this experiment carried out in early summer (**Fig. 8a**). Due to their large cell size compared to other groups accounted for, cryptophytes likely grow slowly (Marañón, 2015; Tang, 1995), which probably accounts for their low numbers throughout the experiment. They could also have been hindered by competition from faster growing cells. The fact that the abundances in the mesocosms were lower than the fjord abundance indicates that the mesocosms created a poor environment for these cells.

The peaks in autotrophic picoeukaryote (APE) abundance (**Fig. 9a**) show that the environment in the mesocosms was favourable for this group. It has long been thought that growth rate decreases with size (Tang, 1995), but recent studies have shown intermediate sizes to have the highest growth rates (reviewed in Marañón, 2015). The APEs grew faster initially than any

other group in this experiment, indicating that the ANEs were either heavily grazed upon or experienced limitations or unfavourable conditions not experienced by the APEs. The rapid decrease in APE abundance after the peak may have been caused by a viral attack, predation, or a combination of these factors (Baudoux, Veldhuis, Witte, & Brussaard, 2007; Evans, Archer, Jacquet, & Wilson, 2003). APE abundances remaining low during the second half of the experiment could have been due to competition and/or predation. Both heterotrophic nanoflagellates (HNFs) and ciliates are known grazers of APEs (Rassoulzadegan et al., 1988; Stockner & Antia, 1986), meaning both groups likely contributed to keeping the APE abundance low.

Synechococcus sp. cells exhibited minimal initial growth and stayed at low abundances for most of the experiment (**Fig. 9b**). They are pico-sized and are thus, together with the heterotrophic bacteria, of the smallest cells included in the current study. Their minimal initial net growth could support the theory that small cells have lower growth rates than intermediately sized cells, though they could have been kept at low abundances due to grazing, competition, or non-favourable conditions. I find the most plausible explanation to be competition (likely from heterotrophic bacteria) or predation since their net growth was much higher towards the end of the experiment when the abiotic environmental conditions were similar, presumably due to less predation or newly available nutrients. Growth of *Synechococcus* sp. after roughly two weeks has been observed in mesocosms due to decreased predation (Agawin, Duarte, & Agustí, 2000). HNFs are the main grazers of pico-sized phototrophs (Agawin et al., 2000; Šimek et al., 1997; Stockner & Antia, 1986). This is supported by our experiment, as the steeper increase in *Synechococcus* sp. abundance (**Fig. 9b**) started when the HNF abundance significantly decreased (**Fig. 11**).

The succession pattern of bacteria (**Fig. 10**) corresponds with mesocosm studies from both the Raunefjord (Segovia et al., 2017) and a Swedish lake (Urrutia-Cordero et al., 2017). HNFs are the main predators also of bacteria (e.g. Fenchel, 1982; Sanders, Porter, Bennett, & DeBiase, 1989), but other factors such as nutrient availability, predation from other organisms (e.g. mixotrophs), and virus activity would also have affected bacterial abundance. By comparing abundance patterns, it can be assumed that HNFs were likely not a major predator of APEs in this experiment, though they could have consumed ANEs in addition to bacteria. As HNFs and ANEs are in the same size category, grazing is more likely to have been from larger organisms like ciliates (Rassoulzadegan et al., 1988).

4.1.2 Was there a difference between treatments?

There was little statistically significant difference between the brownification (Bro) treatments (HuminFeed® additions) during the first ANE abundance peak, but we observed significantly higher ANE abundances in the -Bro mesocosms than the +Bro mesocosms during the second peak (**Fig. 7**). Possible reasons for this could be that ANEs perform badly in low light conditions, or that there was more grazing on ANEs or competition for nutrients in +Bro mesocosms. Studies have shown that ciliates do better in areas of low light and high concentrations of dissolved organic carbon (DOC) (Kammerlander et al., 2016), indicating that ciliates could have been grazing more in the +Bro than the -Bro mesocosms and keeping the abundance low. Peaks at late stages of similar experiments (here observed in -Bro mesocosms only) have previously been observed in mesocosms with high concentrations of N, P, and silicon (Duarte, Agusti, & Agawin, 2000). In our experiment, these nutrients were added to the same concentrations in all mesocosms, so the peak was likely an effect of brownification, not high nutrient concentrations.

The cryptophyte abundance showed little to no reaction to brownification. The mean abundances were similar in both treatments, with the +Bro abundances being slightly higher at some time points (**Fig. 8a**). It has been theorised that brownification favours cryptophytes (Weyhenmeyer, Willén, & Sonesten, 2004), but our results cannot support this theory. Our experiment took place during very low cryptophyte abundances. It is possible an effect would have been observed at bloom concentrations. Other factors such as grazing may also have had a bigger effect than the different Bro treatments.

From day 14, *E. huxleyi* abundance in one of the -Bro mesocosms increased rapidly, reaching 1.68×10^3 cells mL^{-1} at the end of the experiment. There does not appear to be a clear reason for this bloom only happening in one mesocosm. The same mesocosm also had higher abundances of APEs (5.37×10^3 cells mL^{-1} at day 19) and *Synechococcus* sp. cells (1.73×10^4 cells mL^{-1} at day 21) than the other -Bro-dFe mesocosms. This mesocosm could have had lower levels of predation, for example due to a viral attack on the predominant grazers, or possibly higher levels of available nutrients.

The significantly higher APE abundance peak early in the experiment in +Bro mesocosms compared to both -Bro mesocosms and the fjord shows that our artificial brownification created a favourable environment for the APEs (**Fig. 9a**). This could mean that APEs are better at utilizing DOC or better adapted to low light conditions than their competitors, or that

brownification inhibits their main grazers. The latter is less likely, as brownification appeared to favour HNFs (assumed to be grazers of APEs) during the APE peak (**Fig. 11**), did not affect most mixotrophs negatively (see chapter 4.2), and is reported to favour ciliates as well (Kammerlander et al., 2016). This difference between treatments contrasts findings in freshwater studies, where an increase in DOC and decrease in light has been reported to have negative or no effect on the APEs (Drakare, Blomqvist, Bergström, & Jansson, 2003; Rasconi, Gall, Winter, & Kainz, 2015). This could be due to differences in marine and freshwater environments, or our initial addition of nutrients causing a difference from natural conditions. The DOC that leads to brownification in marine environments comes from terrestrial or freshwater runoff (Hedges, Keil, & Benner, 1997), so these microbial communities may have been more adapted to dealing with brownification. It is also likely that the longer time spans in these other studies contributed to the differing results, suggesting that short term studies can show a different picture than long term ones.

Synechococcus sp. abundance means were higher in +Bro than -Bro mesocosms throughout the experiment (**Fig. 9b**), particularly during the small peak at day 8, though this difference was never statistically significant. Armbrust, Bowen, Olson, and Chisholm (1989) explain how *Synechococcus* sp. cell cycles last longer during light limitation, meaning they grow slower. Our results do not show this, indicating that other factors inhibit *Synechococcus* sp. growth in -Bro mesocosms, for example higher levels of predation or competition.

HuminFeed®, the substance added to achieve brownification, contains large amounts of DOC. High bacterial abundances, as observed between day 2 and day 6 (**Fig. 10**), were therefore expected in the +Bro mesocosms since bacteria rely on dissolved organic matter (DOM; includes DOC) to grow (**Fig. 1**) (Azam et al., 1983). Increased bacterial growth due to increased concentrations of DOC, brownification, and temperature have been observed in mesocosm studies previously (Wilken et al., 2018). In our experiment the statistically significant difference between treatments was not due to increased bacterial abundance in the +Bro mesocosms as expected, but due to the high abundances lasting longer. As HNFs rely on bacteria for food, the peak in bacterial abundance could have been the cause of the spike in HNF abundance at day 6 that was not present in -Bro mesocosms (**Fig. 11**). It is possible that the bacterial community in the +Bro mesocosms was more resistant to grazers and/or viruses than that in the -Bro mesocosms. The bacterial community could be adapting to different conditions quickly enough that no effects from the treatments given are observed. As the bacteria were not separated into groups or identified, it is not known how the bacterial community changed throughout the

experiment. The composition of the bacterial community has been shown to change throughout a mesocosm experiment (Riemann, Steward, & Azam, 2000), and bacterial communities are resilient to changing conditions caused by both top-down control and nutrient concentrations (Matz & Jürgens, 2003; Tsagaraki et al., 2018).

The hypothesis that brownification would lead to changes in the composition of the microbial communities was partly supported, as statistically significant changes were observed to some degree for ANEs, APEs, and bacteria, with bacteria showing the least difference between treatments of the three groups.

4.2 Effects of brownification on percentage of mixotrophs

4.2.1 Development of percent LysoTracker positive cells

The general trend in patterns of percent LysoTracker positive cells was that percentages decreased or stayed low for the first half of the experiment, before increasing towards the end (**Fig. 12**). Assuming that mixotrophy is a survival strategy for the cells, this suggests that conditions in the mesocosms grew worse for them over time and more non-constitutive mixotrophs (NCMs) were performing phagotrophy towards the end of the experiment. Mixotrophy could also have been performed as a response to an abundance of nutrients, with cells only then being able to maintain a phagotrophic capability in addition to phototrophy. Similar studies to ours have shown that N and P concentrations decreased rapidly (Egge & Aksnes, 1992; Segovia et al., 2017), meaning the increase in mixotrophic cells was likely a survival mechanism. Though some bacteria perform phagotrophy, *Synechococcus* sp. is only known to be prey through bacterial phagotrophy (Rashidan & Bird, 2001), not a predator. Therefore, there must have been another explanation for the LysoTracker positive *Synechococcus* sp. cells, likely unspecific staining.

Mixotrophic autotrophic nanoeukaryotes (ANEs) are known to be of great importance. They comprise up to 50% of the ANE population and are responsible for >80% of bacterivory in some areas (Havskum & Riemann, 1996; Sanders et al., 1989). Percentages of LysoTracker positive ANE cells started high on day 0 and had been reduced by approximately half by day 2 of the experiment (**Fig. 12a**). This could be the result of suboptimal conditions in the fjord at the time the water was added to the mesocosms, or cells experiencing stress when being pumped into the mesocosms, causing them to resort to phagotrophy. Another possibility is that the strict phototrophs grew faster than the mixotrophs, making the percentage of LysoTracker positive cells decrease. However, predominantly phototrophic mixotrophs, as these cells are assumed

to be, have been reported to have growth rates similar to those of strict phototrophs due to the relatively low cost of maintaining a phagotrophic capability (Raven, 1997). Percent LysoTracker positive ANE cells increased towards the end of the experiment (**Fig. 12a**), coinciding with an increase in abundance, particularly in mesocosms without addition of HuminFeed® (**Fig. 7**). It appears that the cells behaving more phagotrophically made it possible for them to grow, which could mean that mixotrophy in these cells is mainly a survival strategy for poor conditions. This strategy has previously been observed in several nutrient-limited ANEs (Anderson et al., 2018).

The percentages of LysoTracker positive *Emiliania huxleyi* cells starting high on day 0 and then dropping significantly (**Fig. 12d**) could mean that also this particular ANE species uses mixotrophy as a survival strategy and that conditions improved once they were placed in the mesocosms. It could also mean that they turned to phagotrophy due to stress during the pumping of the water into the enclosures. Towards the end of the experiment there was an increase in percent LysoTracker positive cells (**Fig. 12d**), indicating that the conditions turned suboptimal and *E. huxleyi* cells again had to resort to phagotrophy. It is possible that cells only perform phagotrophy under optimal conditions but given the rapid decline in LysoTracker positive cells right after nutrients were added (day 0), this is unlikely. The fact that only a small portion of *E. huxleyi* cells were LysoTracker positive indicates that they are NCMs. This is supported by other studies having observed some, but minimal, phagotrophy in *E. huxleyi* cells (Avrahami & Frada, 2020; Rokitta et al., 2011). The higher percentage of mixotrophs in our study could be due to unspecific staining in the cells or difference in methods.

The percentages of LysoTracker positive cryptophyte cells had wide error bars due to few cells present in the mesocosms (often <20 cells mL^{-1} from day 8, **Fig. 12c**). Anderson et al. (2017) only calculated percentages of mixotrophs when the abundance of a group was >30 cells mL^{-1}, which decreases the chance of a type II error (to not reject a false null hypothesis). Most percentages of LysoTracker positive cryptophytes in our experiment would not have been used when applying this cut-off, so no conclusions should be drawn from these values.

Autotrophic picoeukaryotes (APEs) have also been shown to contribute significantly to bacterivory (Sanders & Gast, 2012; Zubkov & Tarran, 2008), but are less known to be mixotrophic than ANEs. This could be a result of the methods used to determine mixotrophy, as observing ingested particles in pico-sized cells can be challenging, and mixotrophic APEs have been shown to not ingest larger prey (Sanders & Gast, 2012). During the first half of the

experiment, percentage of LysoTracker positive APE cells stayed relatively low, before increasing towards the end of the experiment in all mesocosms (**Fig. 12b**), coinciding with a slight increase in abundance (**Fig. 8a**). This may indicate that the APE population experienced growth towards the end of the experiment due to more cells performing phagotrophy.

Synechococcus sp. showed a trend of increasing percentage of LysoTracker positive cells towards the end of the experiment (**Fig. 12e**). Up to 20% of *Synechococcus* sp. cells in each sample during this experiment were stained, and since *Synechococcus* sp. is not known to perform phagotrophy, this indicates that LysoTracker not only stained food vacuoles. One possible explanation is staining of the thylakoid lumen in chloroplasts, as the pH is similar to that in food vacuoles. Rose et al. (2004) did not find a difference in fluorescent signal between live and dead *Synechococcus* sp. cells, meaning that this is a possibility only if chloroplasts are not destroyed in dead cells. Unspecific staining in *Synechococcus* sp. cells does not necessarily mean that this also occurred in eukaryotic cells, as it is possible that *Synechococcus* sp. cells or cyanobacteria in general interact differently than eukaryotes with the LysoTracker stain.

The F_v/F_m values (optimal quantum yield of photosystem II) were calculated in each mesocosm throughout the experiment and give insight into how healthy the phototrophic cells in the communities were (**Fig. A1**, method in **Appendix A.2**). Normally F_v/F_m values reach about 0.6 in nutrient rich conditions and about 0.3 during nutrient limitation (Crespo, Espinoza-Gonzalez, Teixeira, Castro, & Figueiras, 2011). In the current experiment, the F_v/F_m values started declining at day 6, and percentages of LysoTracker positive cells of most groups started increasing around day 10 or 12 (**Fig. 12**). It is possible that with the chloroplasts yielding less energy, cells needed to perform more phagotrophy. It is also possible that the F_v/F_m values relate little or not at all to mixotrophy, and that the reason that the phototrophs in +Bro mesocosms were less healthy was that the brownification of the water made photosynthesis less effective so cells created more chloroplasts to compensate. The first theory is supported by the fact that even *Synechococcus* sp. cells had an increase in LysoTracker positive cells towards the end of the experiment (**Fig. 12e**), possibly caused by staining of the thylakoid lumen of chloroplasts. As they do not have food vacuoles, the increase must have another cause, for example staining of the thylakoid lumen. There could also have been less nutrients available in the +Bro mesocosms.

4.2.3 Was there a difference between treatments?

The statistically significant difference in percentage of LysoTracker positive ANE cells between treatments towards the end of the experiment indicated that more cells in the -Bro mesocosms were mixotrophic than in the +Bro (brownification) mesocosms (**Fig. 12a**). This contradicted the hypothesis that brownification leads to more mixotrophs. The difference occurred during the second peak in ANE abundance in -Bro mesocosms, possibly indicating that ANE cells resort to phagotrophy due to limited resources, as observed in some ANE species by Anderson et al. (2018). The fact that this difference was observed could be due to the higher abundances of ANEs in -Bro mesocosms causing less nutrients to be available to strict phototrophs. This supports the idea that phagotrophy is a survival strategy for these cells. Another possibility is that there was more competition in +Bro mesocosms, causing more ANEs to not be able to consume bacteria. Since the changes observed due to brownification were not until the last two days of the experiment, it is possible that more changes would have been observed in a longer lasting experiment. Both the cryptophytes and *E. huxleyi* appear to show a trend of higher percentages of LysoTracker positive cells in -Bro mesocosms towards the end of the experiment (**Figs. 12c** and **12d**), supporting these findings.

Increase in APE abundances did not cause a coinciding increase in percentages of LysoTracker positive cells (**Figs. 9a** and **12b**). The significantly higher APE abundances in +Bro mesocosms compared to -Bro mesocosms can therefore not be explained by an increase in cells capable of performing phagotrophy. The mean percentages of LysoTracker positive APE cells in the -Bro and +Bro treatments did not show significant differences (**Fig. 12b**), meaning that brownification did not affect percentages of mixotrophs in this experiment. The same was true for *Synechococcus* sp. Though there were more differences in means for this group (**Fig. 12e**), these differences were not statistically significant due to larger error bars and did not show a clear trend.

Studying the effects of brownification on mixotrophic microorganisms using mesocosms is often done in combination with increasing temperatures (e.g. Urrutia-Cordero et al., 2017; Wilken et al., 2018). This is because brownification and increased concentrations of dissolved organic carbon (DOC) are indirect effects of the increase in runoff caused by higher temperature in predicted future scenarios in lakes and coastal waters (IPCC, 2014; S. Larsen et al., 2011). The results of our study indicate that the effects shown in such studies could be due to a combined effect or an increasing temperature rather than brownification, though studies showing an effect of brownification alone exist (e.g. Lebret et al., 2018). All the aforementioned

studies were performed in freshwater lakes, but parallels can still be made to marine environments, particularly coastal areas, since not only does freshwater affect the oceans due to input of water, but effects could still be similar even in different environments. Coastal areas are expected to be affected due to input of dissolved organic matter (DOM) from rivers and lakes, as observed in Norwegian fjords (Aksnes et al., 2009).

Though the only statistically significant difference between treatments occurred for ANEs, a more general trend of all nano-sized groups (ANEs, cryptophytes, and *E. huxleyi*) appeared, showing a decrease in mixotrophs due to brownification. As this experiment only ran for 21 days, and an increase in mixotrophs was observed only in the second half, it is likely that more pronounced differences would have appeared if the experiment lasted longer. However, the hypothesis could not be supported, as the trends show the opposite effect.

4.3 Effects of iron addition

For phototrophs, iron is an important micronutrient for growth due to its involvement in photosynthesis and assimilation of N (Behrenfeld & Milligan, 2013), as well as to minimise DNA damage (Segovia, Lorenzo, Iñiguez, & García-Gómez, 2018). The North Atlantic is generally not regarded as iron-limited (Behrenfeld et al., 2009), but in some areas *Emiliania huxleyi* may experience iron limitation (Nielsdóttir, Moore, Sanders, Hinz, & Achterberg, 2009; Segovia et al., 2017). Therefore, the overall hypothesis put forward in the BIPWeb project was that addition of dissolved iron (dFe) would promote a bloom of phototrophic plankton, particularly *E. huxleyi*.

The average abundances of both autotrophic nanoeukaryotes (ANEs) (**Fig. A2**) and *E. huxleyi* (**Fig. A3b**) cells appeared to be higher in -dFe mesocosms than +dFe mesocosms, indicating that iron could have had a negative effect on these cells. Partly responsible for this trend was the bloom in one of the -dFe mesocosms. This contrasted both the hypothesis of the project and previous findings that *E. huxleyi* responds positively to dFe addition (Nielsdóttir et al., 2009; Segovia et al., 2017). The cryptophyte abundances did not appear to be affected by the dFe addition, as the means were similar in both treatments (**Fig. A3a**).

Neither autotrophic picoeukaryote (APE) nor *Synechococcus* sp. abundances appeared to be affected by the addition of dFe (**Fig. A4**). *Synechococcus* sp. has previously been reported to be positively affected by dFe in a similar mesocosm experiment (Segovia et al., 2017), and natural APE populations in the Pacific Ocean were stimulated by iron as well (Behrenfeld, Bale, Kolber, Aiken, & Falkowski, 1996). Neither of those experiments included a brownification

effect, so it is possible that the brownification treatment concealed or stopped the positive effects of dFe.

Hutchins, Witter, Butler, and Luther (1999) found that eukaryotic and prokaryotic phototrophs used different strategies to assimilate iron, with eukaryotic species relying more on porphyrin-complexed iron and cyanobacteria relying more on siderophores. This could be part of the reason why dFe appeared to have little effect on abundances of the eukaryotic phototrophs accounted for in this experiment, though it does not explain why our results contradict others. It is possible that any effect of dFe was obscured by the effect of brownification, or that the organisms in the mesocosms simply did not experience iron-limitation.

Bacterial and heterotrophic nanoflagellate (HNF) abundances also appear to have been unaffected by dFe addition (**Figs. A5** and **A6**). The effects of iron on bacterial abundance reported are varied. Some report little to no changes due to iron addition (Church, Hutchins, & Ducklow, 2000; Kirchman et al., 2000), while others report that bacteria are stimulated by addition of iron (Cochlan, 2001; Pakulski et al., 1996). This variation could be due to the area or time of year studies are performed, or the composition of the bacterial population, as different species could respond differently to iron addition or have different needs for iron.

The percentages of LysoTracker positive ANE cells appear to be slightly elevated in +dFe mesocosms (**Fig. A7a**), though not enough to be statistically significant. This trend is not observed for the other nano-sized groups (cryptophytes and *E. huxleyi*; **Figs. A7c** and **A7d**). Both pico-sized groups, APEs (**Fig. A7b**) and *Synechococcus* sp. (**Fig. A7e**), also show a slight increase in LysoTracker positice cells in +Bro mesocosms, but not a statistically significant difference. As previously discussed, *Synechococcus* sp. cannot perform phagotrophy and thus staining of these cells must be unspecific.

It has been shown that ingestion of bacteria in *Ochromonas* sp., a species belonging to the ANEs, can provide large amounts of the iron needed for growth, indicating that mixotrophs are well-adapted to iron-limitation (Maranger, Bird, & Price, 1998). Assuming that bacterivory is not performed solely to acquire iron in these cells, this seems to be supported by our results that show little positive effect from dFe addition to percent LysoTracker positive cells of all groups. If cells already perform bacterivory to meet other needs and acquire iron through this, there is no need to transition into using dFe. Behrenfeld et al. (1996) found that iron enrichment caused the F_v/F_m values to increase exponentially. Our results contradict this, with the -dFe mesocosms having a higher peak than the +dFe mesocosms at the start of the experiment and reaching lower

values towards the end (**Fig. A8**). Our results imply that phototrophs in the -dFe mesocosms were healthier than those in the +dFe mesocosms.

The hypothesis that addition of dFe would affect both the composition of the microbial community and the percentage of mixotrophic phototrophs could not be supported based on the results from this experiment. There are many possible reasons, for example that any effect from dFe was concealed by the effects of brownification or that the water was not iron limited to begin with.

4.4 The LysoTracker method

The method used to determine whether cells were mixotrophic or not was first used by Rose et al. (2004) for enumeration of heterotrophic nanoflagellates (HNFs) in natural samples, and further developed by Sintes and Del Giorgio (2010). It has recently been used to target and identify mixotrophic phototrophs in some studies (Anderson et al., 2018; Anderson et al., 2017; Li et al., 2016), but is still not a widely applied method. In this study the method was used to enumerate mixotrophic phototrophs. I chose to denote these potentially mixotrophic cells "LysoTracker positive cells" since unspecific staining could not be ruled out.

I used a fluorescence microscope to observe how the LysoTracker stain interacted with cells from several cultures and found that it was sometimes unclear whether the stained parts were food vacuoles. Therefore, to examine in more detail how LysoTracker interacts with some algae cells, I investigated cells from cultures of *Dunaliella tertiolecta* K-0591, *Ochromonas* sp., and *Tetraselmis* sp. using confocal microscopy (**Box 5**, method in **Appendix A.3**). *D. tertiolecta* (described as a pure phototroph; Fischer, Giebel, Hillebrand, & Ptacnik, 2017) cells did not take up LysoTracker stain, whereas both *Ochromonas* sp. (a confirmed mixotroph; Pringsheim, 1952) and *Tetraselmis* sp. (a possible mixotroph) cells did (**Fig. 13b**, **13d**). *Ochromonas* sp. cells (**Fig. 13b**) showed a clear line around the cell that indicated staining of the cytoplasmic membrane, and possibly the cytoplasm itself due to staining in some areas inside the cell. In

BOX 5 | Confocal microscopy

Confocal microscopy, also called confocal laser scanning microscopy (CLSM), is an imaging technique that was patented by Marvin Minsky in 1957 and has since become important in many fields, including microbiology (Inoué, 2006). It uses a laser light source and an optical microscope that is connected to a computer with a digital imaging system (Munn, 2011). By focusing the light on a narrow part of the specimen it is possible to create clear images of those slices of specimen (Inoué, 2006). It is also possible to combine such images into a 3D image of for example a cell, and to put brightfield or phase-contrast images next to or superimposed on confocal images (Inoué, 2006). In relation to microbiology, one of the great advantages of confocal microscopy is that it can be used on live cells (Munn, 2011).

some *Ochromonas* sp. cells (like the lower right cell pictured in **Fig. 13b**) there appeared to be an outline of a vacuole or a similar structure, indicating staining of the membrane of a cell structure. This was not as expected, and something that has not been discussed in any other papers (to my knowledge). Wilken et al. (2019) show micrographs of *Ochromonas* CCMP2951 stained with LysoTracker. They observed a clear signal from one part of the cell which is assumed to be a food vacuole. Similar results have been observed in the chlorophyte *Chlamydomonas* sp. ICE-MDV and the haptophyte *Isochrysis* sp. MDV (Li et al., 2016), where a small part of the cell was clearly stained. In our micrographs, *Tetraselmis* sp. cells were stained in large parts of the cells where no chlorophyll fluorescence was observed. I interpret this as a large stained food vacuole, staining of the cytoplasm, or a combination of these due to the large stained area. The chloroplasts in *Tetraselmis* sp. cells did not appear to be stained, as has been theorised can happen (Wilken et al., 2019), since the red colour of the chlorophyll and the green colour of the LysoTracker were well separated.

Though *Ochromonas* sp. is a well-known phagotroph (e.g. Andersson, Falk, Samuelsson, & Hagström, 1989; Pringsheim, 1952), this does not mean that the cells pictured must be mixotrophic. These cells could be non-constitutive mixotrophs (NCMs) and thus not always have food vacuoles present. This is supported by the fact that only one of the cells pictured (lower right cell in **Fig. 13b**) shows the outline of what could be a food vacuole. The pictured *Ochromonas* sp. cells have less chlorophyll (red colour) than the other cells pictured, indicating more efficient chloroplasts, lower demand for energy and nutrients, or them being less reliant on photosynthesis. Whether one of the pictured *Ochromonas* sp. cells show a food vacuole or not, the majority of staining in the pictured cells was unspecific. Anderson et al. (2017) briefly mention that they checked for unspecific binding to structures other than food vacuoles on 12 species of small phytoflagellates (<20 µm). They did not observe unspecific binding, though the method used to examine this was not mentioned. Wilken et al. (2019) observed unspecific staining within a plastid of a cell when using the acidotropic probe LysoSensor that likely resulted from staining of the acidic thylakoid lumen. These differing results means that more work needs to be done to develop this method for use on cells that perform phototrophy, as this use of LysoTracker is a relatively new method and was originally developed for use on strict heterotrophs (Rose et al., 2004).

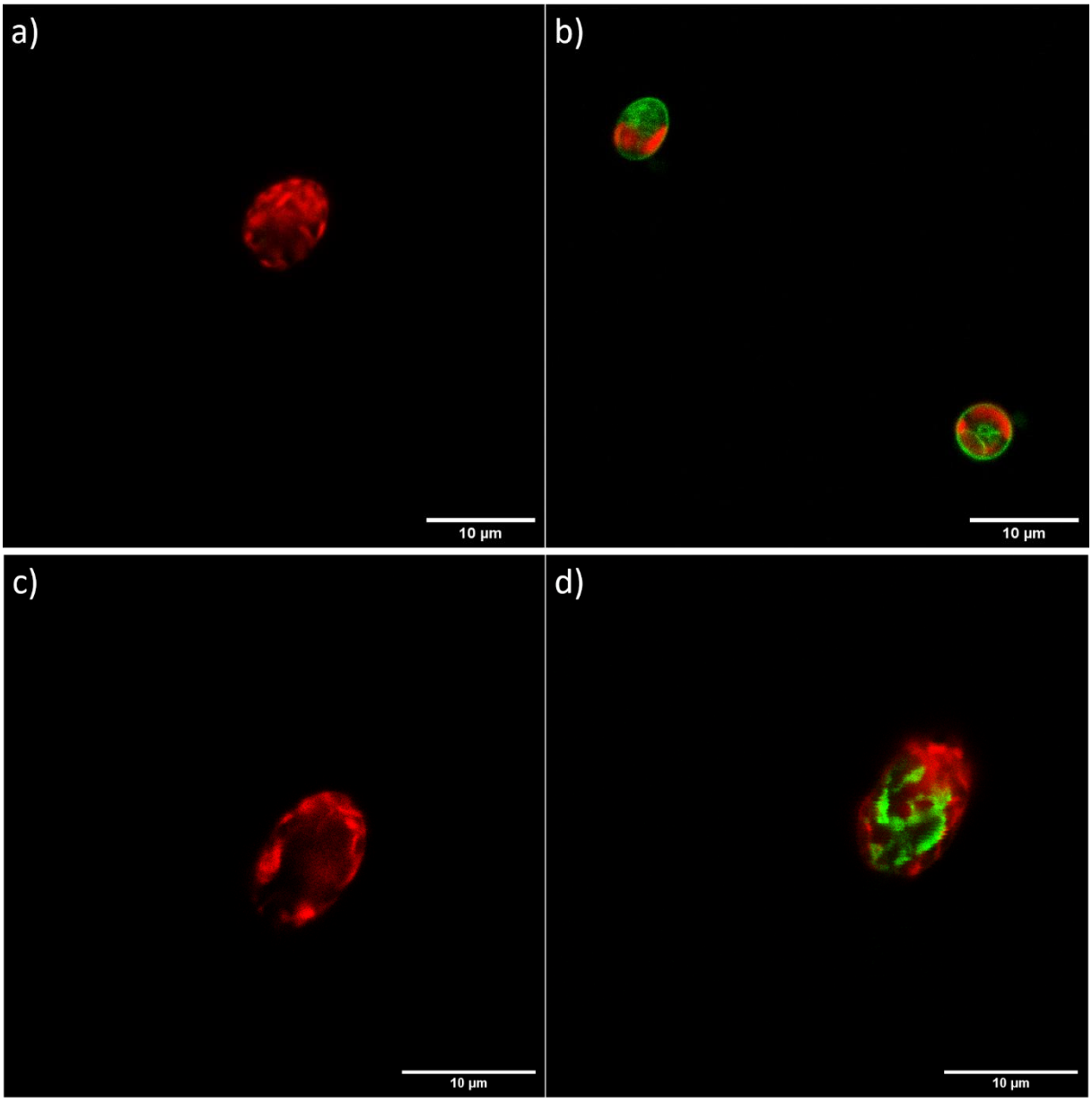

Figure 13. Micrographs taken using confocal microscopy. Chlorophyll is shown in dark red and the acidotropic probe LysoTracker Green in light green. Images show the negative control *Dunaliella* sp. with LysoTracker added (a), the positive control *Ochromonas* sp. with LysoTracker added (b), *Tetraselmis* sp. without added LysoTracker (c), and *Tetraselmis* stained with LysoTracker (d).

Little research has been done to examine how LysoTracker interacts with cell structures like chloroplasts. Wilken et al. (2019) argue that unspecific staining is more likely in phototrophs than strict heterotrophs due to a lack of lumen activity in strict heterotrophs. Considering the LysoTracker methodology was originally developed for use in HNFs (Sintes & Del Giorgio, 2010), then used in mixotrophs without adaptation (Anderson et al., 2017; Li et al., 2016), it is necessary to research the effect of the probe specifically on mixotrophs before establishing the method as common practice.

Due to an error, on day 14 the LysoTracker samples were treated slightly differently than all other days, with the LysoTracker being added to the tubes before the water samples. The normal procedure was to add LysoTracker into the samples already aliquoted into the tubes. Since the percentages of LysoTracker positive cells were higher on day 14 than any other days (**Fig. 12**), I suspect that a homogenous solution was not created when mixing by gently turning the tubes in circles. Using a vortexer would be more damaging to the cells but mix more efficiently, and the protocol by Sintes and Del Giorgio (2010) does in fact include gently vortexing the samples. As samples are collected by the flow cytometer at the bottom of the tubes, it is possible that the percentages on day 14 are the more accurate values. Supporting this theory is the fact that high percentages of mixotrophs (>90%) during early summer have been observed in freshwater lake mesocosms previously (Wilken et al., 2018). It was still assumed that the ratios between days, treatments, and groups were true to life for the rest of the measurements, even though the percentages could be lower (due to a non-homogenous solution) or higher (due to unspecific staining) than the true values.

4.5 Conclusion

Through this mesocosm experiment we were able to observe how brownification led to a change in the composition of the microbial community. Both the autotrophic picoeukaryotes (APEs) and bacteria were positively affected, while autotrophic nanoeukaryotes (ANEs) were negatively affected. The difference between brownification treatments was strongest for ANEs and APEs. Our results imply that microbial communities in future coastal areas with increasing brownification will comprise of fewer ANEs and more APEs, and experience increased bacterial abundances.

Percentages of LysoTracker positive cells, cells assumed to be mixotrophic, was raised in mesocosms without brownification compared to mesocosms with brownification for ANEs at the end of the experiment. The other nano-sized groups (cryptophytes and *Emiliania huxleyi*) also showed this trend. This implies that, contrary to predicted scenarios, brownification leads to fewer phototrophic cells performing phagotrophy.

Though the addition of dissolved iron (dFe) was expected to induce a bloom of *E. huxleyi*, no effect was observed on the composition of the microbial community. Similarly, no significant effect of dFe was observed on percentages of LysoTracker positive cells. Based on these results, it was assumed that cells did not experience iron limitation during this experiment, or that any

effect was obscured by the effect of brownification. Our results could indicate that iron has little effect on mixotrophic activity in a microbial community.

The method using LysoTracker to identify mixotrophs was shown through confocal microscopy to lead to unspecific staining in some of the pictured ANEs. This method should be further developed for use on mixotrophs.

4.6 Future Work

It has become clear that the ongoing climate changes will have a great impact on the oceans and marine communities. Understanding the effects of these changes is already in focus, but the effects on microbial communities are still uncertain. Moving forward with this research it is important not only to focus on the marine microbes, but also to include mixotrophy. Mesocosm studies are invaluable in understanding how marine microbial communities interact and react to different scenarios and will continue to be so moving forward. Most studies on climate change effects (e.g. brownification, increased temperature) relating to aquatic microbes are performed in lakes, but I would argue for a larger focus on marine environments, as recent research has shown these are significantly affected as well.

Future mesocosm studies focusing on mixotrophy should be performed in a range of different environments to investigate if they react differently to expected scenarios. Using molecular methods like sequencing could be beneficial to examine how the community changes as more or fewer mixotrophs are present, or as the environment changes. This could give indications as to who are more mixotrophic, and who are more likely to dominate communities in future environments.

While studies of mesocosms and natural environments provide an overview of the larger picture, laboratory studies are useful for understanding single species. Not many mixotrophs have been studied in detail, so cultivation and examining of such species is still needed to understand how specific species contribute to the larger picture provided by studies of communities. Most studied species are nano-sized, so particularly pico-sized organisms are little understood and need to be studied regarding mixotrophy. By understanding how single species react, it becomes easier both to understand how whole communities react, and to predict how they will react to future scenarios.

When further studying the effects of iron addition on mixotrophic behaviour, it would be beneficial to start investigating effects of iron alone before looking at interactions with other

factors like brownification. Levels of mixotrophy in relation to iron concentrations is a study area with little previous knowledge, so there is much yet to be understood.

References

Adamec, L. (1997). Mineral nutrition of carnivorous plants: a review. *The Botanical Review, 63*(3), 273-299.

Agawin, N. S., Duarte, C. M., & Agustí, S. (2000). Response of Mediterranean Synechococcus growth and loss rates to experimental nutrient inputs. *Marine Ecology Progress Series, 206*, 97-106.

Aksnes, D. L., Dupont, N., Staby, A., Fiksen, Ø., Kaartvedt, S., & Aure, J. (2009). Coastal water darkening and implications for mesopelagic regime shifts in Norwegian fjords. *Marine Ecology Progress Series, 387*, 39-49.

Anderson, R., Charvet, S., & Hansen, P. J. (2018). Mixotrophy in Chlorophytes and Haptophytes—Effect of Irradiance, Macronutrient, Micronutrient and Vitamin Limitation. *Frontiers in microbiology, 9*.

Anderson, R., Jürgens, K., & Hansen, P. J. (2017). Mixotrophic phytoflagellate bacterivory field measurements strongly biased by standard approaches: a case study. *Frontiers in microbiology, 8*, 1398.

Andersson, A., Falk, S., Samuelsson, G., & Hagström, Å. (1989). Nutritional characteristics of a mixotrophic nanoflagellate, Ochromonas sp. *Microbial Ecology, 17*(3), 251-262.

Andersson, A., Haecky, P., & Hagström, Å. (1994). Effect of temperature and light on the growth of micro-nano-and pico-plankton: impact on algal succession. *Marine Biology, 120*(4), 511-520.

Armbrust, E., Bowen, J., Olson, R., & Chisholm, S. (1989). Effect of light on the cell cycle of a marine Synechococcus strain. *Applied and environmental microbiology, 55*(2), 425-432.

Avrahami, Y., & Frada, M. J. (2020). Detection of phagotrophy in the marine phytoplankton group of the coccolithophores (Calcihaptophycidae, Haptophyta) during nutrient-replete and phosphate-limited growth. *Journal of phycology*.

Azam, F., Fenchel, T., Field, J. G., Gray, J., Meyer-Reil, L., & Thingstad, F. (1983). The ecological role of water-column microbes in the sea. *Marine Ecology Progress Series*, 257-263.

Baudoux, A.-C., Veldhuis, M. J., Witte, H. J., & Brussaard, C. P. (2007). Viruses as mortality agents of picophytoplankton in the deep chlorophyll maximum layer during IRONAGES III. *Limnology and oceanography, 52*(6), 2519-2529.

Baumgartner, F. A., Pavia, H., & Toth, G. B. (2015). Acquired phototrophy through retention of functional chloroplasts increases growth efficiency of the sea slug Elysia viridis. *PLoS One, 10*(4), e0120874.

Behrenfeld, M. J., Bale, A. J., Kolber, Z. S., Aiken, J., & Falkowski, P. G. (1996). Confirmation of iron limitation of phytoplankton photosynthesis in the equatorial Pacific Ocean. *Nature, 383*(6600), 508-511.

Behrenfeld, M. J., & Milligan, A. J. (2013). Photophysiological expressions of iron stress in phytoplankton. *Annual Review of Marine Science, 5*, 217-246.

Behrenfeld, M. J., Westberry, T. K., Boss, E. S., O'Malley, R. T., Siegel, D. A., Wiggert, J. D., . . . Doney, S. C. (2009). Satellite-detected fluorescence reveals global physiology of ocean phytoplankton. *Biogeosciences, 6*(5), 779.

Beisner, B. E., Grossart, H.-P., & Gasol, J. M. (2019). A guide to methods for estimating phago-mixotrophy in nanophytoplankton. *Journal of Plankton Research, 41*(2), 77-89.

Biecheler, B. (1936). Observation de la capture et de la digestion des proies chez un Péridinien vert. *CR Séances Soc. Biol, 122*, 1173-1175.

Bird, D. F., & Kalff, J. (1986). Bacterial grazing by planktonic lake algae. *Science, 231*(4737), 493-495.

Bratbak, G., Jacquet, S., Larsen, A., Pettersson, L. H., Sazhin, A. F., & Thyrhaug, R. (2011). The plankton community in Norwegian coastal waters—abundance, composition, spatial distribution and diel variation. *Continental Shelf Research, 31*(14), 1500-1514.

Brutemark, A., & Granéli, E. (2011). Role of mixotrophy and light for growth and survival of the toxic haptophyte Prymnesium parvum. *Harmful Algae, 10*(4), 388-394.

Burkholder, J. M., Glibert, P. M., & Skelton, H. M. (2008). Mixotrophy, a major mode of nutrition for harmful algal species in eutrophic waters. *Harmful Algae, 8*(1), 77-93. doi:https://doi.org/10.1016/j.hal.2008.08.010

Cabrerizo, M. J., González-Olalla, J. M., Hinojosa-López, V. J., Peralta-Cornejo, F. J., & Carrillo, P. (2019). A shifting balance: responses of mixotrophic marine algae to cooling and warming under UVR. *New Phytologist, 221*(3), 1317-1327.

Caron, D. A., Porter, K. G., & Sanders, R. W. (1990). Carbon, nitrogen, and phosphorus budgets for the mixotrophic phytoflagellate Poterioochromonas malhamensis (Chrysophyceae) during bacterial ingestion. *Limnology and oceanography, 35*(2), 433-443.

Carvalho, W. F., & Granéli, E. (2006). Acidotropic probes and flow cytometry: a powerful combination for detecting phagotrophy in mixotrophic and heterotrophic protists. *Aquatic microbial ecology, 44*(1), 85-96.

Church, M. J., Hutchins, D. A., & Ducklow, H. W. (2000). Limitation of bacterial growth by dissolved organic matter and iron in the Southern Ocean. *Applied and environmental microbiology, 66*(2), 455-466.

Cochlan, W. P. (2001). The heterotrophic bacterial response during a mesoscale iron enrichment experiment (IronEx II) in the eastern equatorial Pacific Ocean. *Limnology and oceanography, 46*(2), 428-435.

Cotrim da Cunha, L., Buitenhuis, E. T., Le Quéré, C., Giraud, X., & Ludwig, W. (2007). Potential impact of changes in river nutrient supply on global ocean biogeochemistry. *Global Biogeochemical Cycles, 21*(4).

Crespo, B., Espinoza-Gonzalez, O., Teixeira, I., Castro, C. G., & Figueiras, F. (2011). Possible mixotrophy of pigmented nanoflagellates: Microbial plankton biomass, primary production and phytoplankton growth in the NW Iberian upwelling in spring. *Estuarine, Coastal and Shelf Science, 94*(2), 172-181.

Drakare, S., Blomqvist, P., Bergström, A. K., & Jansson, M. (2003). Relationships between picophytoplankton and environmental variables in lakes along a gradient of water colour and nutrient content. *Freshwater Biology, 48*(4), 729-740.

Duarte, C. M., Agusti, S., & Agawin, N. S. (2000). Response of a Mediterranean phytoplankton community to increased nutrient inputs: a mesocosm experiment. *Marine Ecology Progress Series, 195*, 61-70.

Egge, J. K., & Aksnes, D. (1992). Silicate as regulating nutrient in phytoplankton competition. *Marine ecology progress series. Oldendorf, 83*(2), 281-289.

Egge, J. K., & Heimdal, B. R. (1994). Blooms of phytoplankton including Emiliania huxleyi (Haptophyta). Effects of nutrient supply in different N: P ratios. *Sarsia, 79*(4), 333-348.

Evans, C., Archer, S. D., Jacquet, S., & Wilson, W. H. (2003). Direct estimates of the contribution of viral lysis and microzooplankton grazing to the decline of a Micromonas spp. population. *Aquatic microbial ecology, 30*(3), 207-219.

Fenchel, T. (1982). Ecology of heterotrophic microflagellates. IV. Quantitative occurrence and importance as bacterial consumers. *Mar. Ecol. Prog. Ser, 9*(3), 5.

Field, C. B., Behrenfeld, M. J., Randerson, J. T., & Falkowski, P. (1998). Primary production of the biosphere: integrating terrestrial and oceanic components. *Science, 281*(5374), 237-240.

Figueroa, F. L., Korbee, N., Carrillo Lechuga, P., Medina-Sánchez, J. M., Mata, M., Bonomi, J., & Sánchez-Castillo, P. M. (2009). The effects of UV radiation on photosynthesis estimated as chlorophyll fluorescence in Zygnemopsis decussata (Chlorophyta) growing in a high mountain lake (Sierra Nevada, Southern Spain).

Fischer, R., Giebel, H.-A., Hillebrand, H., & Ptacnik, R. (2017). Importance of mixotrophic bacterivory can be predicted by light and loss rates. *Oikos, 126*(5), 713-722. doi:10.1111/oik.03539

Flynn, K. J., Mitra, A., Anestis, K., Anschütz, A. A., Calbet, A., Ferreira, G. D., . . . Martin, J. L. (2019). Mixotrophic protists and a new paradigm for marine ecology: where does plankton research go now? *Journal of Plankton Research, 41*(4), 375-391.

Flynn, K. J., Stoecker, D. K., Mitra, A., Raven, J. A., Glibert, P. M., Hansen, P. J., . . . Burkholder, J. M. (2013). Misuse of the phytoplankton–zooplankton dichotomy: the need to assign organisms as mixotrophs within plankton functional types. *Journal of Plankton Research, 35*(1), 3-11. doi:10.1093/plankt/fbs062

Gerea, M., Queimaliños, C., Schiaffino, M. R., Izaguirre, I., Forn, I., Massana, R., & Unrein, F. (2012). In situ prey selection of mixotrophic and heterotrophic flagellates in Antarctic oligotrophic lakes: an analysis of the digestive vacuole content. *Journal of Plankton Research, 35*(1), 201-212. doi:10.1093/plankt/fbs085

Godrijan, J., Drapeau, D., & Balch, W. M. (2020). Mixotrophic uptake of organic compounds by coccolithophores. *Limnology and oceanography*.

Harley, C. D., Randall Hughes, A., Hultgren, K. M., Miner, B. G., Sorte, C. J., Thornber, C. S., . . . Williams, S. L. (2006). The impacts of climate change in coastal marine systems. *Ecology letters, 9*(2), 228-241.

Hartmann, M., Grob, C., Tarran, G. A., Martin, A. P., Burkill, P. H., Scanlan, D. J., & Zubkov, M. V. (2012). Mixotrophic basis of Atlantic oligotrophic ecosystems. *Proceedings of the National Academy of Sciences, 109*(15), 5756-5760.

Havskum, H., & Riemann, B. (1996). Ecological importance of bacterivorous, pigmented flagellates (mixotrophs) in the Bay of Aarhus, Denmark. *Marine Ecology Progress Series, 137*, 251-263.

Hedges, J. I., Keil, R. G., & Benner, R. (1997). What happens to terrestrial organic matter in the ocean? *Organic geochemistry, 27*(5-6), 195-212.

Heifetz, P. B., Förster, B., Osmond, C. B., Giles, L. J., & Boynton, J. E. (2000). Effects of Acetate on Facultative Autotrophy inChlamydomonas reinhardtii Assessed by Photosynthetic Measurements and Stable Isotope Analyses. *Plant Physiology, 122*(4), 1439-1446.

Hoppe, H.-G., Breithaupt, P., Walther, K., Koppe, R., Bleck, S., Sommer, U., & Jürgens, K. (2008). Climate warming in winter affects the coupling between phytoplankton and bacteria during the spring bloom: a mesocosm study. *Aquatic microbial ecology, 51*(2), 105-115.

Hutchins, D. A., Witter, A. E., Butler, A., & Luther, G. W. (1999). Competition among marine phytoplankton for different chelated iron species. *Nature, 400*(6747), 858-861.

Inoué, S. (2006). Foundations of confocal scanned imaging in light microscopy. In *Handbook of biological confocal microscopy* (pp. 1-19): Springer.

IPCC. (2014). *Climate Change 2014: Synthesis Report. Contribution of Working Groups I, II and III to the Fifth Assessment Report of the Intergovernmental Panel on Climate Change*. Retrieved from https://www.ipcc.ch/report/ar5/syr/

Jacquet, S., Heldal, M., Iglesias-Rodriguez, D., Larsen, A., Wilson, W., & Bratbak, G. (2002). Flow cytometric analysis of an Emiliana huxleyi bloom terminated by viral infection. *Aquatic microbial ecology, 27*(2), 111-124.

Jeong, H. J., Yoo, Y. D., Kim, J. S., Seong, K. A., Kang, N. S., & Kim, T. H. (2010). Growth, feeding and ecological roles of the mixotrophic and heterotrophic dinoflagellates in marine planktonic food webs. *Ocean Science Journal, 45*(2), 65-91. doi:10.1007/s12601-010-0007-2

Jickells, T. (1998). Nutrient biogeochemistry of the coastal zone. *Science, 281*(5374), 217-222.

Jones, R. I. (2000). Mixotrophy in planktonic protists: an overview. *Freshwater Biology, 45*(2), 219-226.

Kammerlander, B., Koinig, K. A., Rott, E., Sommaruga, R., Tartarotti, B., Trattner, F., & Sonntag, B. (2016). Ciliate community structure and interactions within the planktonic food web in two alpine lakes of contrasting transparency. *Freshwater Biology, 61*(11), 1950-1965.

Kassambara, A. (n.d.). Mixed ANOVA in R. Retrieved from https://www.datanovia.com/en/lessons/mixed-anova-in-r/

Kirchman, D. L., Meon, B., Cottrell, M. T., Hutchins, D. A., Weeks, D., & Bruland, K. W. (2000). Carbon versus iron limitation of bacterial growth in the California upwelling regime. *Limnology and oceanography, 45*(8), 1681-1688.

Kritzberg, E., & Ekström, S. (2012). Increasing iron concentrations in surface waters-a factor behind brownification? *Biogeosciences, 9*(4), 1465.

Larsen, A., Castberg, T., Sandaa, R., Brussaard, C., Egge, J., Heldal, M., . . . Bratbak, G. (2001). Population dynamics and diversity of phytoplankton, bacteria and viruses in a seawater enclosure. *Marine Ecology Progress Series, 221*, 47-57.

Larsen, A., Flaten, G. A. F., Sandaa, R.-A., Castberg, T., Thyrhaug, R., Erga, S. R., . . . Bratbak, G. (2004). Spring phytoplankton bloom dynamics in Norwegian coastal waters: microbial community succession and diversity. *Limnology and oceanography, 49*(1), 180-190.

Larsen, S., Andersen, T., & Hessen, D. O. (2011). Climate change predicted to cause severe increase of organic carbon in lakes. *Global Change Biology, 17*(2), 1186-1192.

Lebaron, P., Servais, P., Troussellier, M., Courties, C., Vives-Rego, J., Muyzer, G., . . . Stackebrandt, E. (1999). Changes in bacterial community structure in seawater mesocosms differing in their nutrient status. *Aquatic microbial ecology, 19*(3), 255-267.

Lebret, K., Langenheder, S., Colinas, N., Östman, Ö., & Lindström, E. S. (2018). Increased water colour affects freshwater plankton communities in a mesocosm study. *Aquatic microbial ecology, 81*(1), 1-17.

Li, W., Podar, M., & Morgan-Kiss, R. M. (2016). Ultrastructural and single-cell-level characterization reveals metabolic versatility in a microbial eukaryote community from an ice-covered Antarctic lake. *Applied and environmental microbiology, 82*(12), 3659-3670.

Liu, Z., Campbell, V., Heidelberg, K. B., & Caron, D. A. (2016). Gene expression characterizes different nutritional strategies among three mixotrophic protists. *FEMS microbiology ecology, 92*(7), fiw106.

Madigan, M. T., Bender, K. S., Buckley, D. H., Sattley, W. M., & Stahl, D. A. (2019). *Brock Biology of Microorganisms* (Global fifteenth ed.). Harlow, England: Pearson Education.

Maranger, R., Bird, D., & Price, N. (1998). Iron acquisition by photosynthetic marine phytoplankton from ingested bacteria. *Nature, 396*(6708), 248.

Marañón, E. (2015). Cell size as a key determinant of phytoplankton metabolism and community structure.

Marie, D., Partensky, F., Vaulot, D., & Brussaard, C. (1999). Enumeration of phytoplankton, bacteria, and viruses in marine samples. *Current protocols in cytometry, 10*(1), 11.11. 11-11.11. 15.

Marie, D., Simon, N., & Vaulot, D. (2005). Phytoplankton cell counting by flow cytometry. *Algal culturing techniques, 1*, 253-267.

Marrase, C., Lim, E. L., & Caron, D. A. (1992). Seasonal and daily changes in bacterivory in a coastal plankton community. *Marine Ecology Progress Series*, 281-289.

Matz, C., & Jürgens, K. (2003). Interaction of nutrient limitation and protozoan grazing determines the phenotypic structure of a bacterial community. *Microbial Ecology, 45*(4), 384-398.

Medina-Sánchez, J. M., Felip, M., & Casamayor, E. O. (2005). Catalyzed reported deposition-fluorescence in situ hybridization protocol to evaluate phagotrophy in mixotrophic protists. *Applied and environmental microbiology, 71*(11), 7321-7326.

Mitra, A., Flynn, K. J., Burkholder, J. M., Berge, T., Calbet, A., Raven, J. A., . . . Stoecker, D. K. (2014). The role of mixotrophic protists in the biological carbon pump. *Biogeosciences, 11*(4), 995-1005.

Mitra, A., Flynn, K. J., Tillmann, U., Raven, J. A., Caron, D., Stoecker, D. K., . . . Sanders, R. (2016). Defining planktonic protist functional groups on mechanisms for energy and nutrient acquisition: incorporation of diverse mixotrophic strategies. *Protist, 167*(2), 106-120.

Munn, C. (2011). *Marine Microbiology: Ecology and Applications* (Second ed.). New York, USA: Garland Science.

Nielsdóttir, M. C., Moore, C. M., Sanders, R., Hinz, D. J., & Achterberg, E. P. (2009). Iron limitation of the postbloom phytoplankton communities in the Iceland Basin. *Global Biogeochemical Cycles, 23*(3).

Nygaard, K., & Tobiesen, A. (1993). Bacterivory in algae: a survival strategy during nutrient limitation. *Limnology and oceanography, 38*(2), 273-279.

Odum, E. P. (1984). The mesocosm. *BioScience, 34*(9), 558-562.

Olson, R. J., Chisholm, S. W., Zettler, E. R., & Armbrust, E. V. (1990). Pigments, size, and distributions of Synechococcus in the North Atlantic and Pacific Oceans. *Limnology and oceanography, 35*(1), 45-58.

Olson, R. J., Zettler, E., & Anderson, O. (1989). Discrimination of eukaryotic phytoplankton cell types from light scatter and autofluorescence properties measured by flow cytometry. *Cytometry: The Journal of the International Society for Analytical Cytology, 10*(5), 636-643.

Pakulski, J. D., Coffin, R. B., Kelley, C. A., Holder, S. L., Downer, R., Aas, P., . . . Jeffrey, W. H. (1996). Iron stimulation of Antarctic bacteria. *Nature, 383*(6596), 133-134.

Pascher, A. (1917). *Flagellaten und Rhizopoden in ihren gegenseitigen Beziehungen: Versuch einer Ableitung der Rhizopoden*.

Paulino, A. I., Egge, J., & Larsen, A. (2008). Effects of increased atmospheric CO 2 on small and intermediate sized osmotrophs during a nutrient induced phytoplankton bloom.

Paulino, A. I., Larsen, A., Bratbak, G., Evens, D., Erga, S. R., Bye-Ingebrigtsen, E., & Egge, J. K. (2018). Seasonal and annual variability in the phytoplankton community of the Raunefjord, west coast of Norway from 2001–2006. *Marine Biology Research, 14*(5), 421-435.

Pitta, P., & Giannakourou, A. (2000). Planktonic ciliates in the oligotrophic Eastern Mediterranean: vertical, spatial distribution and mixotrophy. *Marine Ecology Progress Series, 194*, 269-282.

Pozdnyakov, D. V., Johannessen, O. M., Korosov, A. A., Pettersson, L. H., Grassl, H., & Miles, M. W. (2007). Satellite evidence of ecosystem changes in the White Sea: A semi-enclosed arctic marginal shelf sea. *Geophysical Research Letters, 34*(8).
Pringsheim, E. (1952). On the nutrition of Ochromonas. *Journal of Cell Science, 3*(21), 71-96.
Randall, G. W., & Mulla, D. J. (2001). Nitrate nitrogen in surface waters as influenced by climatic conditions and agricultural practices. *Journal of Environmental Quality, 30*(2), 337-344.
Rasconi, S., Gall, A., Winter, K., & Kainz, M. J. (2015). Increasing water temperature triggers dominance of small freshwater plankton. *PLoS One, 10*(10), e0140449.
Rashidan, K., & Bird, D. (2001). Role of predatory bacteria in the termination of a cyanobacterial bloom. *Microbial Ecology, 41*(2), 97-105.
Rassoulzadegan, F., Laval-Peuto, M., & Sheldon, R. (1988). Partitioning of the food ration of marine ciliates between pico-and nanoplankton. *Hydrobiologia, 159*(1), 75-88.
Raven, J. (1997). Phagotrophy in phototrophs. *Limnology and oceanography, 42*(1), 198-205.
Riemann, L., Steward, G. F., & Azam, F. (2000). Dynamics of bacterial community composition and activity during a mesocosm diatom bloom. *Applied and environmental microbiology, 66*(2), 578-587.
Rokitta, S. D., de Nooijer, L. J., Trimborn, S., de Vargas, C., Rost, B., & John, U. (2011). TRANSCRIPTOME ANALYSES REVEAL DIFFERENTIAL GENE EXPRESSION PATTERNS BETWEEN THE LIFE-CYCLE STAGES OF EMILIANIA HUXLEYI (HAPTOPHYTA) AND REFLECT SPECIALIZATION TO DIFFERENT ECOLOGICAL NICHES 1. *Journal of phycology, 47*(4), 829-838.
Rose, J. M., Caron, D. A., Sieracki, M. E., & Poulton, N. (2004). Counting heterotrophic nanoplanktonic protists in cultures and aquatic communities by flow cytometry. *Aquatic microbial ecology, 34*(3), 263-277.
Rothhaupt, K. O. (1996). Utilization of substitutable carbon and phosphorus sources by the mixotrophic chrysophyte Ochromonas sp. *Ecology, 77*(3), 706-715.
Sanders, R. W. (1991). Mixotrophic protists in marine and freshwater ecosystems. *The Journal of protozoology, 38*(1), 76-81.
Sanders, R. W., & Gast, R. J. (2012). Bacterivory by phototrophic picoplankton and nanoplankton in Arctic waters. *FEMS microbiology ecology, 82*(2), 242-253.
Sanders, R. W., & Porter, K. G. (1988). Phagotrophic phytoflagellates. In *Advances in microbial ecology* (pp. 167-192): Springer.
Sanders, R. W., Porter, K. G., Bennett, S. J., & DeBiase, A. E. (1989). Seasonal patterns of bacterivory by flagellates, ciliates, rotifers, and cladocerans in a freshwater planktonic community. *Limnology and oceanography, 34*(4), 673-687.
Santoferrara, L. F., Guida, S., Zhang, H., & McManus, G. B. (2014). De novo transcriptomes of a mixotrophic and a heterotrophic ciliate from marine plankton. *PLoS One, 9*(7), e101418.
Segovia, M., Lorenzo, M. R., Iñiguez, C., & García-Gómez, C. (2018). Physiological stress response associated with elevated CO2 and dissolved iron in a phytoplankton community dominated by the coccolithophore Emiliania huxleyi. *Marine Ecology Progress Series, 586*, 73-89.
Segovia, M., Lorenzo, M. R., Maldonado, M. T., Larsen, A., Berger, S. A., Tsagaraki, T. M., . . . Palma, A. (2017). Iron availability modulates the effects of future CO2 levels within the marine planktonic food web. *Marine Ecology Progress Series, 565*, 17-33.
Šimek, K., Hartman, P., Nedoma, J., Pernthaler, J., Springmann, D., Vrba, J., & Psenner, R. (1997). Community structure, picoplankton grazing and zooplankton control of heterotrophic nanoflagellates in a eutrophic reservoir during the summer phytoplankton maximum. *Aquatic microbial ecology, 12*(1), 49-63.

Sintes, E., & Del Giorgio, P. A. (2010). Community heterogeneity and single-cell digestive activity of estuarine heterotrophic nanoflagellates assessed using lysotracker and flow cytometry. *Environmental microbiology, 12*(7), 1913-1925.
Sommer, U., Aberle, N., Engel, A., Hansen, T., Lengfellner, K., Sandow, M., . . . Riebesell, U. (2007). An indoor mesocosm system to study the effect of climate change on the late winter and spring succession of Baltic Sea phyto-and zooplankton. *Oecologia, 150*(4), 655-667.
Sosik, H. M., Olson, R. J., & Armbrust, E. V. (2010). Flow Cytometry in Phytoplankton Research. In D. J. Suggett, O. Prášil, & M. A. Borowitzka (Eds.), *Chlorophyll a Fluorescence in Aquatic Sciences: Methods and Applications* (pp. 171-185). Dordrecht: Springer Netherlands.
Stockner, J. G., & Antia, N. J. (1986). Algal picoplankton from marine and freshwater ecosystems: a multidisciplinary perspective. *Canadian journal of fisheries and aquatic sciences, 43*(12), 2472-2503.
Stoecker, D. K., Hansen, P. J., Caron, D. A., & Mitra, A. (2017). Mixotrophy in the Marine Plankton. *Annual Review of Marine Science, 9*(1), 311-335. doi:10.1146/annurev-marine-010816-060617
Suttle, C. A. (2005). Viruses in the sea. *Nature, 437*(7057), 356-361.
Tang, E. P. (1995). The allometry of algal growth rates. *Journal of Plankton Research, 17*(6), 1325-1335.
Tarran, G. A., & Bruun, J. T. (2015). Nanoplankton and picoplankton in the Western English Channel: abundance and seasonality from 2007–2013. *Progress in Oceanography, 137*, 446-455.
The Editors of Encyclopaedia Britannica. (2019). Antonie van Leeuwenhoek. Retrieved from https://www.britannica.com/biography/Antonie-van-Leeuwenhoek
Tranvik, L. J., Porter, K. G., & Sieburth, J. M. (1989). Occurrence of bacterivory in Cryptomonas, a common freshwater phytoplankter. *Oecologia, 78*(4), 473-476.
Tsagaraki, T. M., Pree, B., Leiknes, Ø., Larsen, A., Bratbak, G., Øvreås, L., . . . Olsen, Y. (2018). Bacterial community composition responds to changes in copepod abundance and alters ecosystem function in an Arctic mesocosm study. *The ISME journal, 12*(11), 2694.
Tyrrell, T., & Merico, A. (2004). Emiliania huxleyi: bloom observations and the conditions that induce them. In *Coccolithophores* (pp. 75-97): Springer.
Unrein, F., Gasol, J. M., Not, F., Forn, I., & Massana, R. (2014). Mixotrophic haptophytes are key bacterial grazers in oligotrophic coastal waters. *The ISME journal, 8*(1), 164.
Unrein, F., Massana, R., Alonso-Sáez, L., & Gasol, J. M. (2007). Significant year-round effect of small mixotrophic flagellates on bacterioplankton in an oligotrophic coastal system. *Limnology and oceanography, 52*(1), 456-469.
Urrutia-Cordero, P., Ekvall, M. K., Ratcovich, J., Soares, M., Wilken, S., Zhang, H., & Hansson, L. A. (2017). Phytoplankton diversity loss along a gradient of future warming and brownification in freshwater mesocosms. *Freshwater Biology, 62*(11), 1869-1878.
Walther, G.-R., Post, E., Convey, P., Menzel, A., Parmesan, C., Beebee, T. J., . . . Bairlein, F. (2002). Ecological responses to recent climate change. *Nature, 416*(6879), 389-395.
Ward, B. A., & Follows, M. J. (2016). Marine mixotrophy increases trophic transfer efficiency, mean organism size, and vertical carbon flux. *Proceedings of the National Academy of Sciences, 113*(11), 2958-2963. doi:10.1073/pnas.1517118113
Weithoff, G., & Wacker, A. (2007). The mode of nutrition of mixotrophic flagellates determines the food quality for their consumers. *Functional ecology, 21*(6), 1092-1098.

Weyhenmeyer, G. A., Willén, E., & Sonesten, L. (2004). Effects of an extreme precipitation event on water chemistry and phytoplankton in the Swedish Lake Mälaren. *Boreal Environment Research, 9*(5), 409-420.

Wilken, S., Huisman, J., Naus-Wiezer, S., & Van Donk, E. (2013). Mixotrophic organisms become more heterotrophic with rising temperature. *Ecology letters, 16*(2), 225-233.

Wilken, S., Soares, M., Urrutia-Cordero, P., Ratcovich, J., Ekvall, M. K., Van Donk, E., & Hansson, L. A. (2018). Primary producers or consumers? Increasing phytoplankton bacterivory along a gradient of lake warming and browning. *Limnology and oceanography, 63*(S1), S142-S155.

Wilken, S., Yung, C. C., Hamilton, M., Hoadley, K., Nzongo, J., Eckmann, C., . . . Worden, A. Z. (2019). The need to account for cell biology in characterizing predatory mixotrophs in aquatic environments. *Philosophical Transactions of the Royal Society B, 374*(1786), 20190090.

Worden, A. Z., Follows, M. J., Giovannoni, S. J., Wilken, S., Zimmerman, A. E., & Keeling, P. J. (2015). Rethinking the marine carbon cycle: factoring in the multifarious lifestyles of microbes. *Science, 347*(6223), 1257594.

Young, E. B., & Beardall, J. (2003). Photosynthetic function in Dunaliella tertiolecta (Chlorophyta) during a nitrogen starvation and recovery cycle. *Journal of phycology, 39*(5), 897-905.

Zubkov, M. V., Burkill, P. H., & Topping, J. N. (2007). Flow cytometric enumeration of DNA-stained oceanic planktonic protists. *Journal of Plankton Research, 29*(1), 79-86.

Zubkov, M. V., & Tarran, G. A. (2008). High bacterivory by the smallest phytoplankton in the North Atlantic Ocean. *Nature, 455*(7210), 224.

Appendix A: Methods

A.1 Flow cytometry settings

Table A1. Settings on the flow cytometer (Attune NxT Acoustic Focusing Cytometer, Thermo Fisher Scientific) when counting algae. The same settings were used with and without LysoTracker. FSC = forward scatter, SSC = side scatter, BL1, BL2, and BL3 = detectors that measure output from the 488 nm laser (blue light), YL1, YL2, YL3, and YL4 = detectors that measure output from the 561 nm laser (yellow light).

Acquired volume (µl)	2000
Flow rate (µl/min)	500
Parameter	**Corresponding voltage (mV)**
FSC	350
SSC	240
BL1	260
BL2	320
BL3	370
YL1	400
YL2	400
YL3	400
YL4	400
Threshold	
OR BL3	0.5 (x1,000)

Table A2. Settings for the flow cytometer (Attune NxT Acoustic Focusing Cytometer, Thermo Fisher Scientific) when counting bacteria. FSC = forward scatter, SSC = side scatter, BL1, BL2, and BL3 = detectors that measure output from the 488 nm laser (blue light), YL1, YL2, YL3, and YL4 = detectors that measure output from the 561 nm laser (yellow light).

Acquired volume (µl)	500 (1,000x, 500x, 100x) 200 (50x, 10x) 100 (5x)
Flow rate (µl/min)	500 (1,000x, 500x, 100x) 200 (50x, 10x) 100 (5x)
Parameter	**Corresponding voltage (mV)**
FSC	350
SSC	500
BL1	420
BL2	480
BL3	320
YL1	340
YL2	400
YL3	240
YL4	400
Threshold	
AND SSC	0.2 (x1,000)
AND BL1	0.4 (x1,000)

Table A3. Settings on the flow cytometer (Attune NxT Acoustic Focusing Cytometer, Thermo Fisher Scientific) when counting HNFs. FSC = forward scatter, SSC = side scatter, BL1, BL2, and BL3 = detectors that measure output from the 488 nm laser (blue light), YL1 = detector that measure output from the 561 nm laser (yellow light).

Acquired volume (µl)	2500
Flow rate (µl/min)	500
Parameter	**Corresponding voltage (mV)**
FSC	350
SSC	400
BL1	250
BL2	400
BL3	400
YL1	400
Threshold	
AND SSC	0.1 (x1,000)
AND BL1	1.0 (x1,000)

A.2 F_v/F_m

The optimal quantum yield (F_v/F_m) of photosystem II (PSII) in the phototrophs' chloroplasts was measured by María Segovia and her team in the BIPWeb project (https://coccosphere.es/bipweb/) according to Segovia et al. (2018). This was done on 10 min dark-adapted samples by pulse amplitude modulated fluorometry (Water-PAM, Walz). F_v is the difference between the maximum fluorescence from fully reduced PSII reaction centres (F_m) and the minimum fluorescence (F_O) that occurs in fully oxidised PSII reaction centres (Baumgartner et al., 2015; Figueroa et al., 2009).

A.3 Confocal microscopy

Using cultures available at the Department of Biological Sciences at UiB (chlorophytes *Dunaliella tertiolecta* K-0591 and *Tetraselmis* sp., and the chrysophyte *Ochromonas* sp.), micrographs were taken of several mixotrophic species with the probe LysoTracker® Green DND-26. 100 µL LysoTracker Green was added to 1 mL of culture and incubated for 10 minutes. Then the sample was looked at and taken micrographs of using a confocal microscope (Leica TCS SP8 STED 3x, performed at Molecular Imaging Centre at Institute of Biomedicine at University of Bergen).

Appendix B: Results

B.1 F_v/F_m

The mean F_v/F_m value for the -Bro treatment spanned from $4.13\times10^{-1} \pm 1.39\times10^{-2}$ to $5.16\times10^{-1} \pm 8.63\times10^{-3}$ (**Fig. A1**). It started at $4.69\times10^{-1} \pm 1.02\times10^{-2}$ at day 0, then increased until day 6, at $5.16\times10^{-1} \pm 8.63\times10^{-3}$. From day 6 it decreased until day 19, at $4.13\times10^{-1} \pm 1.39\times10^{-2}$, and ended at $4.20\times10^{-1} \pm 1.23\times10^{-2}$. For the +Bro treatment, the mean F_v/F_m value ranged from $3.46\times10^{-1} \pm 2.90\times10^{-2}$ to $5.24\times10^{-1} \pm 7.39\times10^{-3}$. From a value of 4.72×10^{-1} 4.54×10^{-3} at day 0, it increased to $5.24\times10^{-1} \pm 7.39\times10^{-3}$ at day 6. There was then a decrease until day 19, at $3.46\times10^{-1} \pm 2.90\times10^{-2}$, and it ended at $3.56\times10^{-1} \pm 1.51\times10^{-2}$ at day 21. The mean F_v/F_m value for the fjord spanned from $3.35\times10^{-1} \pm 2.20\times10^{-2}$ to 4.78×10^{-1}. It started at 4.75×10^{-1} at day 0, and from a mean of 4.78×10^{-1} at day 2 it decreased until day 4, at $4.36\times10^{-1} \pm 4.00\times10^{-3}$. From day 6, at $4.52\times10^{-1} \pm 1.15\times10^{-2}$, there was a decrease until day 16, at $3.35\times10^{-1} \pm 2.20\times10^{-2}$, then an increase until the end of the experiment, with a mean F_v/F_m value of $4.55\times10^{-1} \pm 3.35\times10^{-2}$ at day 21.

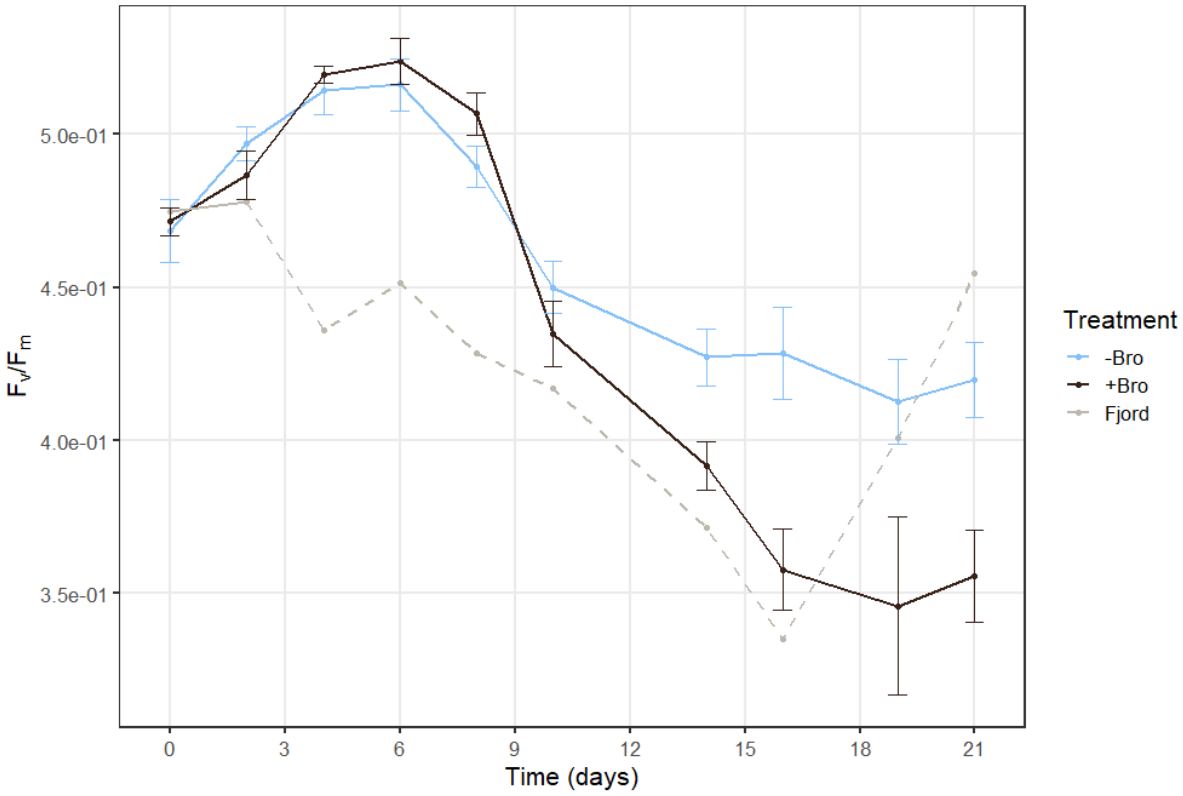

Figure A1. F_v/F_m mean values ±SE throughout the experiment for both the -Bro (blue line) and +Bro (brown line) treatments, and the fjord sample (dashed grey line). n=3 for day 0 and day 2 and n=6 for day 4 to day 21 for the -Bro and +Bro treatments, and n=1 for day 0 and day 2 and n=2 for day 4 to day 21 for the fjord.

B.2 Effect of iron treatment

If no SE is given, only one sample was collected. Sampling of the fjord started at day 6.

B.2.1 Abundances of microbial groups

B.2.1.1 Autotrophic nanoeukaryotes

The mean abundance of ANEs started at 1.50×10^3 cells mL^{-1} at day 0 for both the -dFe and the +dFe treatments (**Fig. A2**). The -dFe treatment mean spanned from $8.75\times10^2 \pm 4.98\times10^1$ cells mL^{-1} to $3.54\times10^3 \pm 1.03\times10^3$ cells mL^{-1}. There were peaks at day 6 at $3.05\times10^3 \pm 1.11\times10^2$ cells mL^{-1}, and at day 19 at $3.54\times10^3 \pm 1.03\times10^3$ cells mL^{-1}. There was also a smaller peak at day 12 at $1.35\times10^3 \pm 5.19\times10^2$ cells mL^{-1}. The +dFe treatment mean ranged from 6.74×10^2 7.03×10^1 cells mL^{-1} to $2.57\times10^3 \pm 1.57\times10^2$ cells mL^{-1}. There was a peak at day 6 at $2.57\times10^3 \pm 1.57\times10^2$ cells mL^{-1}, and another at day 19 at $2.24\times10^3 \pm 6.11\times10^2$ cells mL^{-1}. The fjord abundance spanned from 7.13×10^2 cells mL^{-1} to 4.92×10^3 cells mL^{-1}. It started at 1.26×10^3 cells mL^{-1} at day 6, peaked at day 10 at 4.17×10^3 cells mL^{-1} and from an abundance of 7.13×10^2 cells mL^{-1} at day 16 it increased until the end of the experiment, at 4.92×10^3 cells mL^{-1}.

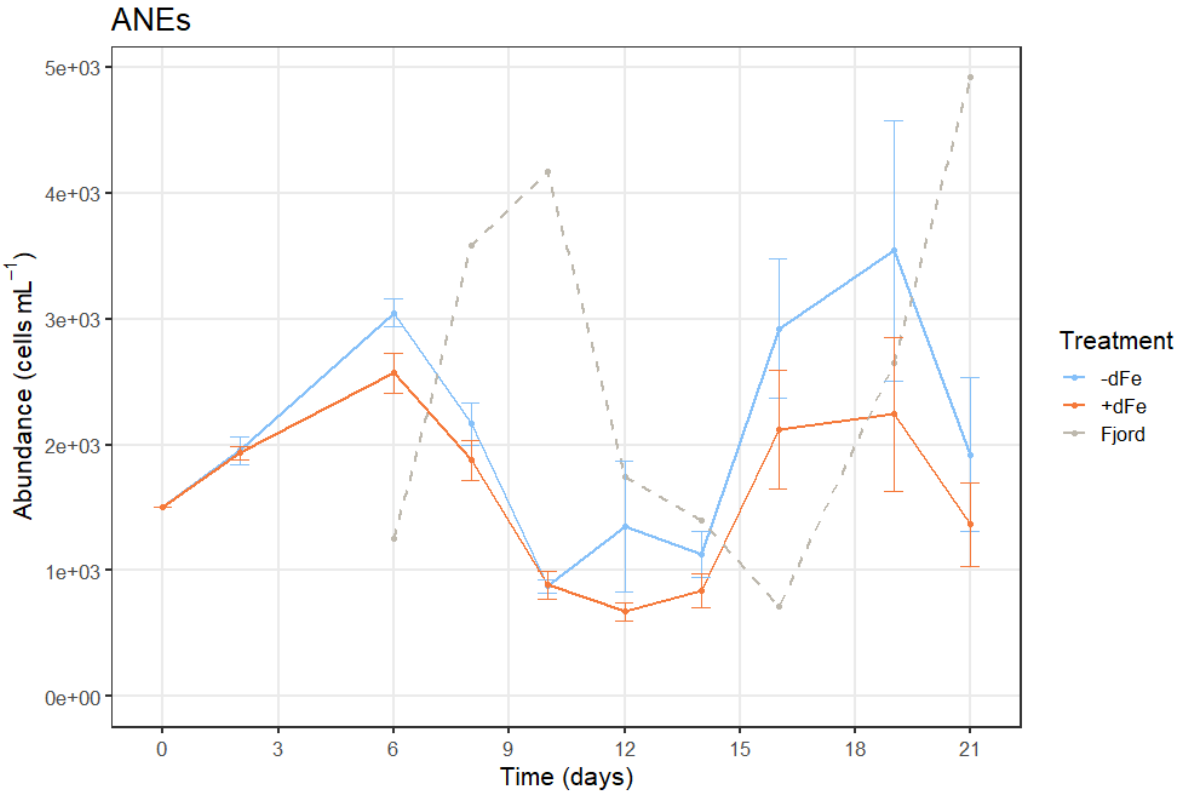

Figure A2. Abundance (cells mL^{-1}) of ANEs on each sample day of the experiment. The dashed grey line shows the abundance in the fjord, while the orange and blue lines show the mean ± SE with and without dFe, respectively. n=6 for both the -dFe and +dFe treatments (days 2-21), n=1 for the fjord, n=1 for day 0.

B.2.1.2 Cryptophytes and *Emiliania huxleyi*

The abundance of cryptophytes at day 0 was 1.22×10^{2} cells mL^{-1} for both the -dFe and the +dFe treatment (**Fig. A3a**). The -dFe treatment had mean abundances spanning from $7.83\times10^{0} \pm 1.64\times10^{0}$ cells mL^{-1} to $1.58\times10^{2} \pm 1.83\times10^{1}$ cells mL^{-1}. There was a peak at day 2 at $1.58\times10^{2} \pm 1.83\times10^{1}$ cells mL^{-1}, then a decrease until day 10 at $7.83\times10^{0} \pm 1.64\times10^{0}$ cells mL^{-1} and an increase from day 10 until the end of the experiment, with an abundance of $4.00\times10^{1} \pm 5.65\times10^{0}$ cells mL^{-1}. The +dFe treatment mean spanned from $6.00\times10^{0} \pm 1.37\times10^{0}$ cells mL^{-1} to $1.53\times10^{2} \pm 1.29\times10^{1}$ cells mL^{-1}. It peaked at day 2 at $1.53\times10^{2} \pm 1.29\times10^{1}$ cells mL^{-1}, decreased until day 14 at $6.00\times10^{0} \pm 1.37\times10^{0}$ cells mL^{-1}, and then increased until the end of the experiment, at $2.50\times10^{1} \pm 6.89\times10^{0}$ cells mL^{-1}. The fjord abundance spanned from 5.30×10^{1} cells mL^{-1} to 3.09×10^{2} cells mL^{-1}. It started at 1.86×10^{2} cells mL^{-1} at day 6, then had two peaks: one at day 10 at 3.09×10^{2} cells mL^{-1}, and one at day 14 at 2.75×10^{2} cells mL^{-1}. From an abundance of from 5.30×10^{1} cells mL^{-1} at day 19 it increased until day 21 at 2.23×10^{2} cells mL^{-1}.

The mean abundance of *E. huxleyi* at day 0 was 5.10×10^{2} cells mL^{-1} for both the -dFe and the +dFe treatment (**Fig. A3b**). The -dFe treatment mean spanned from $1.38\times10^{2} \pm 3.79\times10^{1}$ cells mL^{-1} to $5.17\times10^{2} \pm 5.99\times10^{1}$ cells mL^{-1}. It had a peak at day 8 at $5.17\times10^{2} \pm 5.99\times10^{1}$ cells mL^{-1}, then decreased until day 14 at $1.38\times10^{2} \pm 3.79\times10^{1}$ cells mL^{-1}. From day 14 there was an increase until the end of the experiment, at $3.55\times10^{2} \pm 2.65\times10^{2}$ cells mL^{-1}, with SEs of $>1.62\times10^{2}$ for day 16, 19, and 21. The mean abundance for the +dFe treatment spanned from $6.53\times10^{1} \pm 1.52\times10^{1}$ cells mL^{-1} to 5.10×10^{2} cells mL^{-1}. From day 0 there was a decrease until day 2 at $3.08\times10^{2} \pm 1.47\times10^{1}$ cells mL^{-1}, then a peak at day day 8 at $3.93\times10^{2} \pm 4.23\times10^{1}$ cells mL^{-1}. From day 14, at $6.53\times10^{1} \pm 1.52\times10^{1}$ cells mL^{-1}, there was an increase until the end of the experiment, at $1.36\times10^{2} \pm 4.95\times10^{1}$ cells mL^{-1}. The fjord abundance spanned from 5.20×10^{1} cells mL^{-1} to 6.30×10^{2} cells mL^{-1}. It started at 6.30×10^{2} cells mL^{-1} at day 6, decreased until day 19 at 5.20×10^{1} cells mL^{-1}, and from day 19 it increased until day 21 at 7.30×10^{1} cells mL^{-1}.

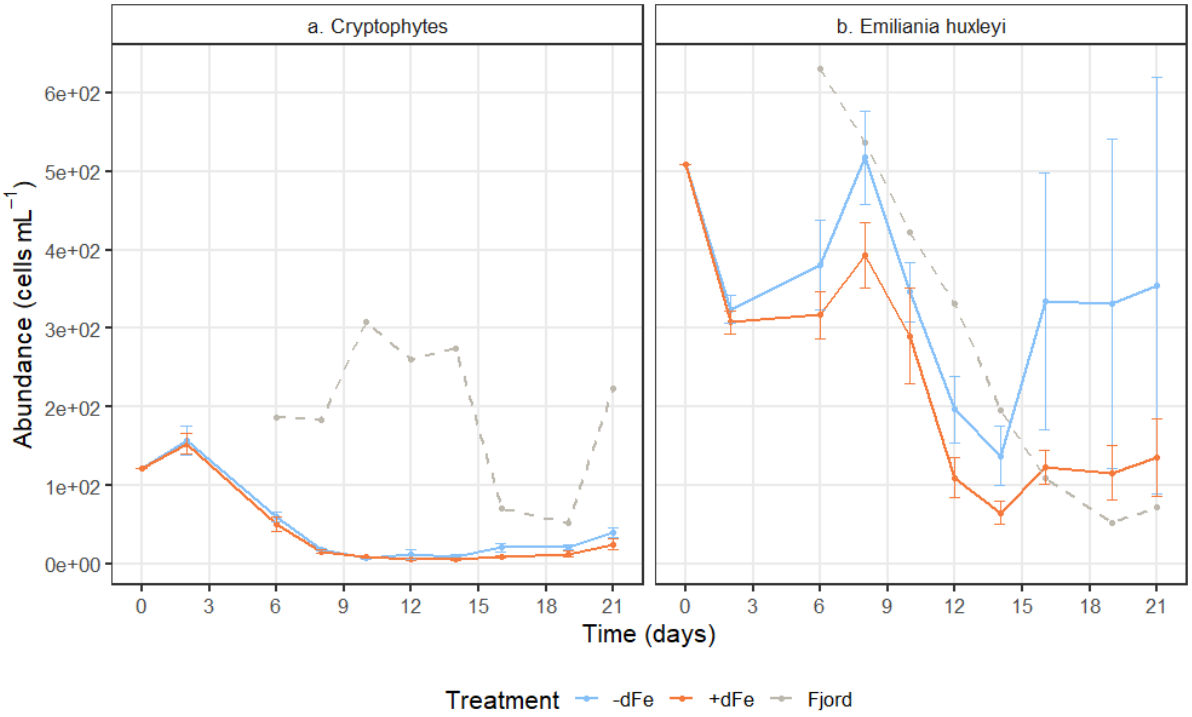

Figure A3. Abundance (cells mL^{-1}) of cryptophytes (a) and *E. huxleyi* (b) on each sample day of the experiment. The dashed grey line shows the abundance in the fjord, while the orange and blue lines show the mean ± SE with and without dFe, respectively. n=6 for both the -dFe and +dFe treatments (days 2-21), n=1 for the fjord, n=1 for day 0.

B.2.1.3 Autotrophic picoeukaryotes

The mean abundance of APEs started at 4.08×10^3 cells mL^{-1} for both the -dFe and the +dFe treatments (**Fig. A4a**). The -dFe treatment spanned from $1.37\times10^3 \pm 3.43\times10^2$ cells mL^{-1} to $4.68\times10^4 \pm 1.02\times10^4$ cells mL^{-1}. There was a peak at day 8 at $4.68\times10^4 \pm 1.02\times10^4$ cells mL^{-1}, and from day 10 the mean abundance stayed at $<4.80\times10^3$ cells mL^{-1}. The abundance mean for the +dFe treatment spanned from $1.99\times10^3 \pm 6.99\times10^2$ cells mL^{-1} to $4.28\times10^4 \pm 1.09\times10^4$ cells mL^{-1}. It peaked at day 8 at $4.28\times10^4 \pm 1.09\times10^4$ cells mL^{-1}, and from day 10 stayed at $<6.70\times10^3$ cells mL^{-1}. The fjord abundance started at 1.50×10^3 cells mL^{-1} at day 6, and spanned from 6.22×10^2 cells mL^{-1} to 1.34×10^4 cells mL^{-1}, peaking at day 10 at 1.34×10^4 cells mL^{-1}. From an abundance of 6.22×10^2 cells mL^{-1} at day 16, it increased until the end of the experiment to 9.45×10^3 cells mL^{-1}.

Both the -dFe and the +dFe abundance of *Synechococcus* sp. started at 9.54×10^3 cells mL^{-1} (**Fig. A4b**). The -dFe abundance mean spanned from $2.88\times10^3 \pm 7.20\times10^2$ cells mL^{-1} to $2.38\times10^4 \pm 5.77\times10^3$ cells mL^{-1}. Until day 8, at $1.10\times10^4 \pm 2.60\times10^3$ cells mL^{-1}, there was a slight increase in the abundance mean, and then it decreased until day 14 at an abundance of $2.88\times10^3 \pm 7.20\times10^2$ cells mL^{-1} before increasing until the end of the experiment, at $2.38\times10^4 \pm 5.77\times10^3$ cells mL^{-1}. The +dFe abundance mean spanned from $2.50\times10^3 \pm 7.54\times10^2$ cells mL^{-1} to

$2.56\times10^4 \pm 7.04\times10^3$ cells mL^{-1}. From day 2 at $1.23\times10^4 \pm 2.28\times10^2$ cells mL^{-1} it decreased until day 12 at $2.50\times10^3 \pm 7.54\times10^2$ cells mL^{-1}. It then increased until the end of the experiment, at $2.56\times10^4 \pm 7.04\times10^3$ cells mL^{-1}. The fjord abundance spanned from 1.00×10^4 cells mL^{-1} to 4.47×10^4 cells mL^{-1}. It started at 1.39×10^4 cells mL^{-1} at day 6, and reached a peak at day 10 at 4.47×10^4 cells mL^{-1}. It then decreased until day 16 at 1.00×10^4 cells mL^{-1} before increasing until the end of the experiment, at 2.93×10^4 cells mL^{-1}.

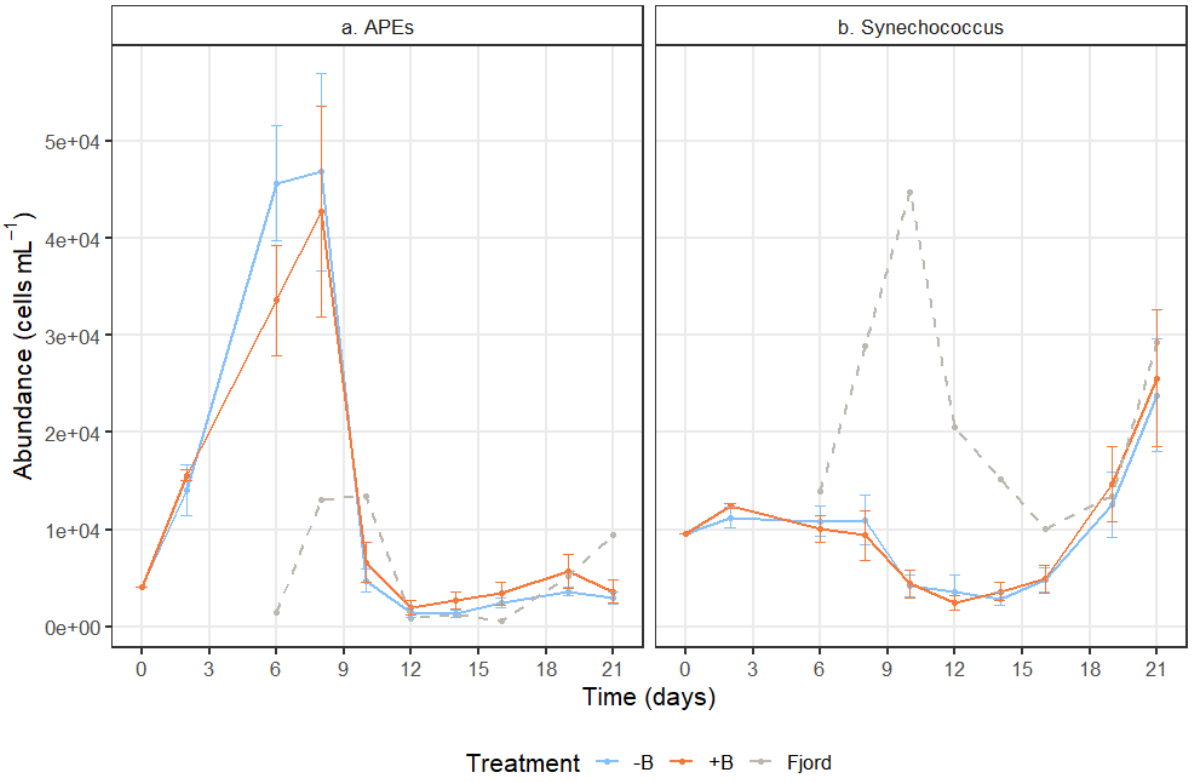

Figure A4. Abundance (cells mL^{-1}) of APEs (a) and *Synechococcus* sp. (b) on each sample day of the experiment. The dashed grey line shows the abundance in the fjord, while the orange and blue lines show the mean ± SE with and without dFe, respectively. n=6 for both the -dFe and +dFe treatments (days 2-21), n=1 for the fjord, n=1 for day 0.

B.2.1.4 Bacteria

For both the -dFe and the +dFe treatments the mean abundance of bacteria started at 8.88×10^5 cells mL^{-1} (**Fig. A5**). The -dFe treatment mean spanned from $4.72\times10^5 \pm 6.13\times10^4$ cells mL^{-1} to $1.22\times10^6 \pm 3.64\times10^4$ cells mL^{-1}. There was a peak at day 2 at $1.22\times10^6 \pm 3.64\times10^4$ cells mL^{-1}, then a decrease until day 10 at $5.01\times10^5 \pm 7.53\times10^4$ cells mL^{-1}. A smaller peak at $6.22\times10^5 \pm 1.11\times10^5$ cells mL^{-1} was present at day 12, and from day 16 at $4.72\times10^5 \pm 6.13\times10^4$ cells mL^{-1} there was an increase until day 21, at 8.02×10^5 3.64×10^4 cells mL^{-1}. The mean for the +dFe treatment spanned from $4.09\times10^5 \pm 5.46\times10^4$ cells mL^{-1} to $1.14\times10^6 \pm 2.09\times10^4$ cells mL^{-1}. It peaked at day 2 at $1.14\times10^6 \pm 2.09\times10^4$ cells mL^{-1} and then decreased until day 12 at

$4.86\times10^5 \pm 3.50\times10^4$ cells mL^{-1}. There was a smaller peak at $5.79\times10^5 \pm 4.85\times10^4$ cells mL^{-1} at day 14, a decrease to $4.09\times10^5 \pm 5.46\times10^4$ cells mL^{-1} at day 16, and then an increase to $7.23\times10^5 \pm 1.22\times10^5$ cells mL^{-1} at the end of the experiment. The fjord abundance spanned from 3.99×10^5 cells mL^{-1} to 9.73×10^5 cells mL^{-1}. It started at 9.73×10^5 cells mL^{-1} at day 6, and decreased until day 8 at 7.05×10^5 cells mL^{-1}. It had a peak at day 12 at 9.45×10^5 cells mL^{-1}, then decreased until day 19 at 3.99×10^5 cells mL^{-1} before increasing to 4.98×10^5 cells mL^{-1} at day 21.

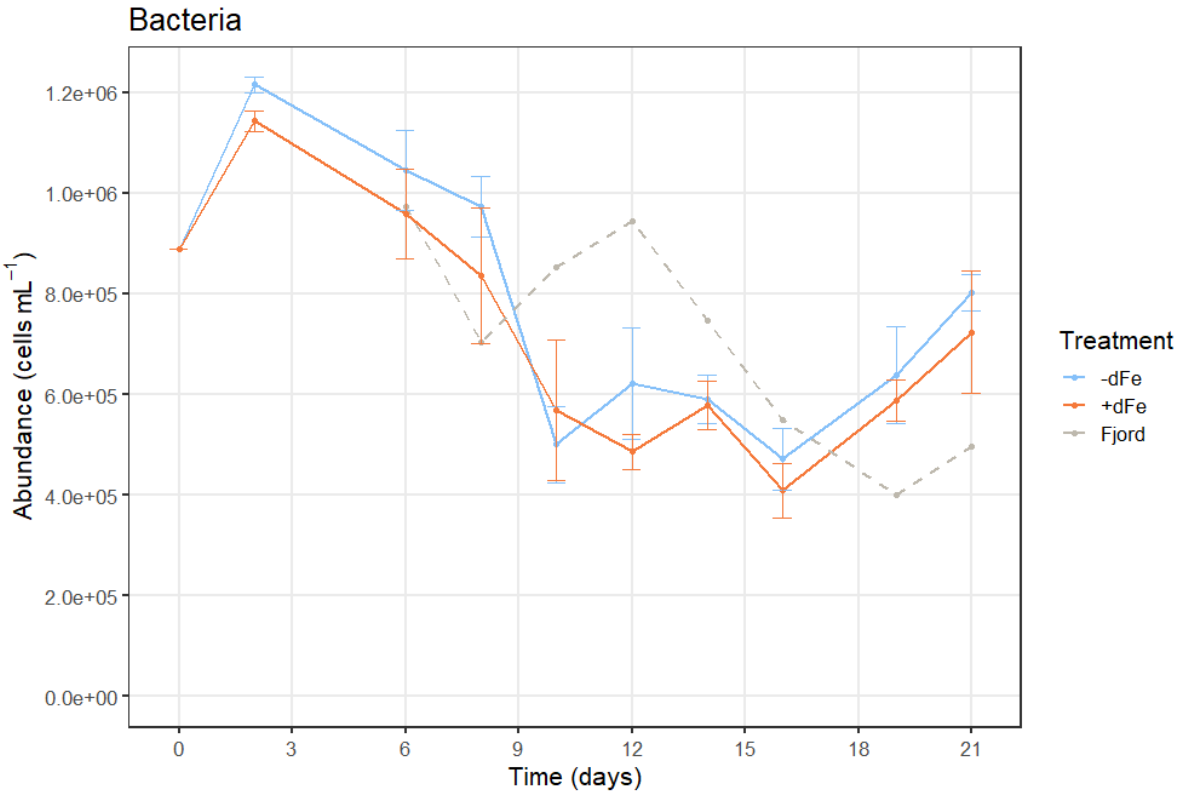

Figure A5. Bacterial abundance (cells mL^{-1}) on each sample day of the experiment. The dashed grey line shows the abundance in the fjord, while the orange and blue lines show the mean ± SE with and without dFe, respectively. n=6 for both the -dFe and +dFe treatments (days 2-21), n=1 for the fjord, n=1 for day 0.

B.2.1.5 Heterotrophic nanoflagellates

The mean abundance of HNFs for both the -dFe and the +dFe treatments was 1.02×10^3 cells mL^{-1} at day 0 (**Fig. A6**). The -dFe treatment mean spanned from $8.68\times10^2 \pm 1.01\times10^2$ cells mL^{-1} to $3.01\times10^3 \pm 2.44\times10^2$ cells mL^{-1}. It had two peaks: one at day 6 at $1.95\times10^3 \pm 2.43\times10^2$ cells mL^{-1}, and one at day 16 at $3.01\times10^3 \pm 2.44\times10^2$ cells mL^{-1}. Between the peaks it decreased to $8.68\times10^2 \pm 1.01\times10^2$ cells mL^{-1} at day 10, and after the second peak there was a decrease until the end of the experiment, at $1.32\times10^3 \pm 1.76\times10^2$. The +dFe treatment mean spanned from $8.24\times10^2 \pm 1.33\times10^2$ cells mL^{-1} to $2.64\times10^3 \pm 3.74\times10^2$ cells mL^{-1}. It peaked both at day 6 and day 16, at $1.98\times10^3 \pm 2.22\times10^2$ cells mL^{-1} and $2.64\times10^3 \pm 3.74\times10^2$ cells mL^{-1}, respectively. After the first peak the mean decreased to $8.24\times10^2 \pm 1.33\times10^2$ cells mL^{-1} at day

10, and after the second peak it decreased until day 19 at $1.10\times10^3 \pm 1.09\times10^2$ cells mL^{-1}, before increasing until day 21 at $1.40\times10^3 \pm 2.46\times10^2$ cells mL^{-1}. The abundance in the fjord spanned from 3.93×10^2 cells mL^{-1} to 2.26×10^3 cells mL^{-1}. It started at 1.15×10^3 cells mL^{-1} at day 6, and had a peak at day 12 at 2.26×10^3 cells mL^{-1}. It then decreased to 3.93×10^2 cells mL^{-1} at day 16, before increasing to 6.71×10^2 cells mL^{-1} at the end of the experiment.

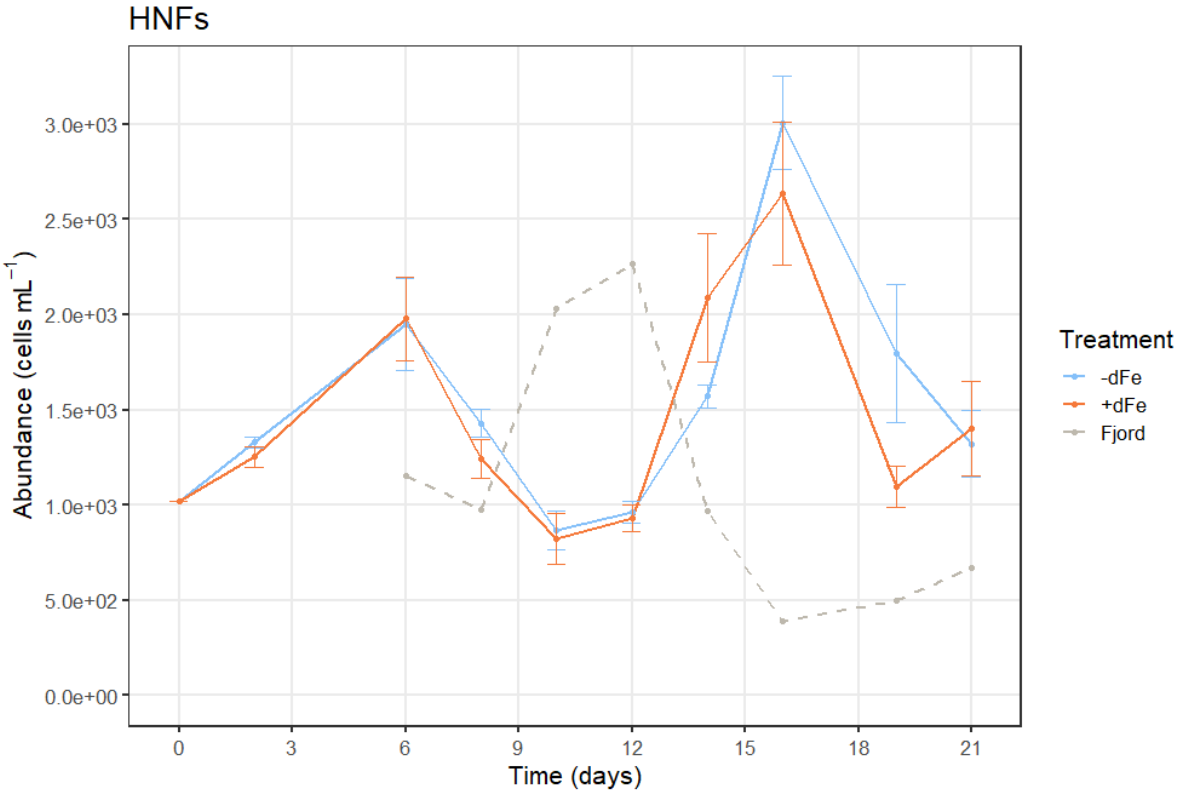

Figure A6. Abundance (cells mL^{-1}) of HNFs on each sample day of the experiment. The dashed grey line shows the abundance in the fjord, while the orange and blue lines show the mean ± SE with and without dFe, respectively. n=6 for both the -dFe and +dFe treatments (days 2-21), n=1 for the fjord, n=1 for day 0.

B.2.2 Percentages of LysoTracker positive cells

B.2.2.1 Autotrophic nanoeukaryotes

The percentage of LysoTracker positive ANE cells at day 0 was 56% for both the -dFe and the +dFe treatment (**Fig. A7a**). The -dFe percentage spanned between 14% ± 1.2% and 56%. From day 0 there was a decrease until day 2, at 21% ± 3.8%, and from day 6, at 22% ± 0.67% there was a further decrease until day 10, at 14 ± 1.2%. There was then a peak at day 19 at 54% ± 2.8%. The +dFe percentage spanned between 20% ± 5.2% and 56%. There was a decrease from day 0 to day 10, at 20% ± 5.2%, then a peak at day 19 at 50% ± 6.6%. The fjord percentage ranged from 6.3% to 61%. It started at 6.3% at day 6, had a peak at 25% at day 8, another peak at day 12 at 18%, and a last peak at day 19 at 61%. At day 14 the -dFe treatment mean was 66% ± 2.4%, the +dFe treatment mean was 65% ± 3.2%, and the fjord mean was 18%.

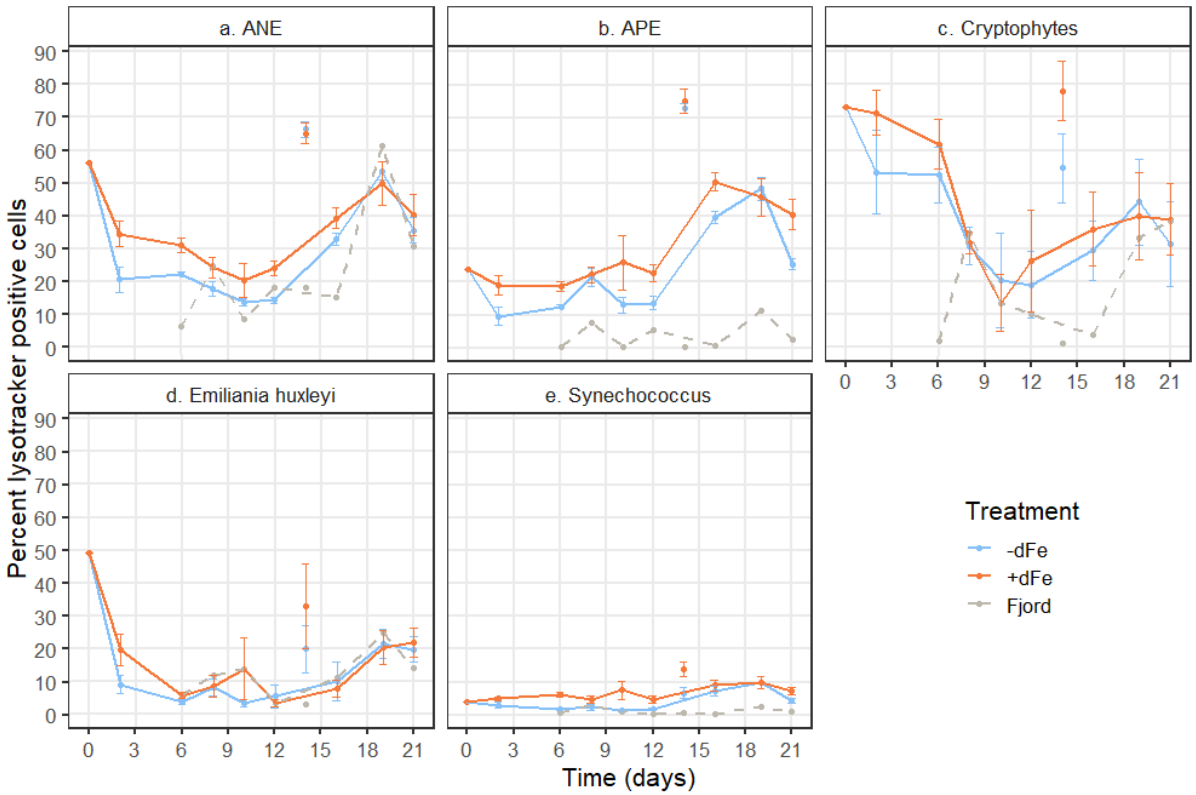

Figure A7. Percentages of LysoTracker positive cells on each sample day of the experiment for each group; ANEs (a), APEs (b), cryptophytes (c), *E. huxleyi* (d), and *Synechococcus* sp. (e). The grey lines show the fjord percentage, while the orange and blue lines show the mean percentage ± SE with and without dFe, respectively. The points on day 14 show the mean percentage ± SE when an error was made when preparing the samples. n=6 for both the -dFe and +dFe treatments (days 2-21), n=1 for the fjord, n=1 for day 0.

B.2.2.2 Cryptophytes and *Emiliania huxleyi*

For the cryptophytes, the mean percentage of LysoTracker positive cells was 73% at day 0 for both the -dFe and the +dFe treatment (**Fig. A7c**). The -dFe treatment mean spanned from 19% ± 10% to 73%. From day 0 there was a decrease until day 12 at 19% ± 10%. There was then an increase until a peak at day 19, at 44% ±13%. The +dFe treatment mean spanned from 14% ± 8.8% to 73%. From day 0 there was a decrease until day 10, at 14% ± 8.8%, then an increase until day 19, at 40% ± 13%, and ending at 39% ± 11% at day 21. The fjord percentage ranged from 2.1% to 38%. It started at 2.1% at day 6, then had a peak at day 8 at 35%, and decreased until day 16 at 3.9%. After day 16 there was an increase until the end of the experiment, at 38%. At day 14 the -dFe treatment percentage mean was 55 ± 10%, the +dFe treatment percentage mean was 78% ± 9.1%, and the fjord percentage was 1.2%.

For *E. huxleyi*, the mean percentage of LysoTracker positive cells was 49% at day 0 for both the -dFe and the +dFe treatment (**Fig. A7d**). The -dFe treatment mean spanned from 3.5% ± 1.2% to 49%. From day 0 it decreased until day 6, at 3.9% ± 0.77%, then there was a small peak at day 8 at 8.3% ± 2.6%. From day 10, at 3.5% ± 1.2%, there was an increase until a peak

at day 19 at 21% ± 4.4%, and it ended at 20% ± 3.9% at day 21. The +dFe treatment mean spanned from 3.4% ± 1.1% to 49%. From day 0 there was a decrease until day 8, at 8.8% ± 3.3%, then a peak at day 10, at 14% ± 9.5%. From day 12, at 3.4 ± 1.1%, there was an increase until the end of the experiment, at 22% ± 4.4%. The fjord percentage ranged between 3.4% and 25%. It started at 5.9% at day 6, increased to a peak at day 10 at 14%, and from day 12, at 3.4%, there was an increase to another peak at day 19 at 25%. It ended at 14% at day 21. At day 14 the -dFe treatment percentage mean was 20% ± 7.2%, the +dFe treatment percentage mean was 33% ± 13%, and the fjord percentage was 3.3%.

B.2.2.3 Autotrophic picoeukaryotes

The mean percentage of LysoTracker positive APE cells at day 0 was 24% for both the -dFe and the +dFe treatment (**Fig. A7b**). The -dFe treatment mean ranged from 9.6% ± 2.7% to 48% ± 3.6%. From day 0 it decreased until day 2 at 9.6% ± 2.7%. There was a small peak at day 8 at 22% ± 2.9%, and from day 10 at 13% ± 2.5% there was an increase until a peak at day 19 at 48% ± 3.6%. The +dFe treatment mean ranged from 19% ± 1.5% to 51% ± 2.9%. From day 0 there was a slight decrease until day 6 at 19% ± 1.5%, and a peak at day 16 at 51% ± 2.9%. From the peak there was a decrease until the end of the experiment, at 40% ± 4.6%. The fjord percentage spanned from 0.31% to 11%. There were peaks at day 8, 12, and 19, at 7.5%, 5.4%, and 11%, respectively. Between the peaks the percentage was at <0.8%, and at day 21 it was at 2.5%. At day 14 the -dFe treatment percentage mean was 73% ± 1.6%, the +dFe treatment percentage mean was 75% ± 3.6%, and the fjord percentage was 0.41%.

The mean percentage of LysoTracker positive *Synechococcus* sp. cells at day 0 was 3.9% for both the -dFe and the +dFe treatment (**Fig. A7e**). The -dFe treatment spanned from 1.4% ± 0.25% to 9.8% ± 1.9%. From day 0 it decreased until day 6, at 1.7% ± 0.14%. From day 8, at 2.4% ± 0.91%, there was a decrease until day 10, at 1.4% ± 0.25%, then a peak at day 19 at 9.8% ± 1.9%. It ended at 4.2% ± 0.73% at day 21. The +dFe treatment ranged from 3.9% to 9.8% ± 2.0%. From day 0 there was an increase until day 6, at 6.1 ± 0.78%, and from day 8, at 4.6% ± 1.2%, it increased to a peak at day 10, at 7.5% ± 2.8%. From day 12, at 4.7% ± 1.2%, there was an increase until a peak at day 19, at 9.8% ± 2.0%. It ended at 7.3 ± 1.1% at day 21. At day 14, the -dFe treatment percentage mean was 6.7% ± 1.6%, the +dFe treatment percentage mean was 14% ± 2.3%, and the fjord percentage was 0.55%.

B.2.3 F_v/F_m

The mean F_v/F_m values for the -dFe treatment spanned from 3.89×10^{-1} ± 1.37×10^{-2} to 5.41×10^{-1} ± 4.43×10^{-3} (**Fig. A8**). It started at day 0 at 4.63×10^{-1} ± 8.08×10^{-3}, then had a peak at

day 6 at $5.41\times10^{-1} \pm 4.43\times10^{-3}$. From day 6 there was a decrease until day 16, at $3.89\times10^{-1} \pm 1.37\times10^{-2}$, then a small peak an increase until day 19, at $4.11\times10^{-1} \pm 2.53\times10^{-2}$, before ending at $4.04\times10^{-1} \pm 1.41\times10^{-2}$ at the end of the experiment. The mean F_v/F_m values for the +dFe treatment spanned from $3.47\times10^{-1} \pm 2.03\times10^{-2}$ to $5.05\times10^{-1} \pm 4.87\times10^{-3}$. It started at 4.77×10^{-1} at day 0, and increased until day 4, at $5.05\times10^{-1} \pm 4.87\times10^{-3}$. From day 8, at 5.04×10^{-1}, there was a decrease until day 19, at $3.47\times10^{-1} \pm 2.03\times10^{-2}$, then an increase until day 21, at $3.72\times10^{-1} \pm 1.79\times10^{-2}$. The fjord mean F_v/F_m values ranged from $3.35\times10^{-1} \pm 2.20\times10^{-2}$ to 4.78×10^{-1}. It started at 4.75×10^{-1} at day 0, and from a value of 4.78×10^{-1} at day 2, there was a decrease until day 4, at $4.36\times10^{-1} \pm 4.00\times10^{-3}$. From day 6, at $4.52\times10^{-1} \pm 1.15\times10^{-2}$, there was a decrease until day 16, at $3.35\times10^{-1} \pm 2.20\times10^{-2}$, then an increase until the end of the experiment, when the value was $4.55\times10^{-1} \pm 3.35\times10^{-2}$.

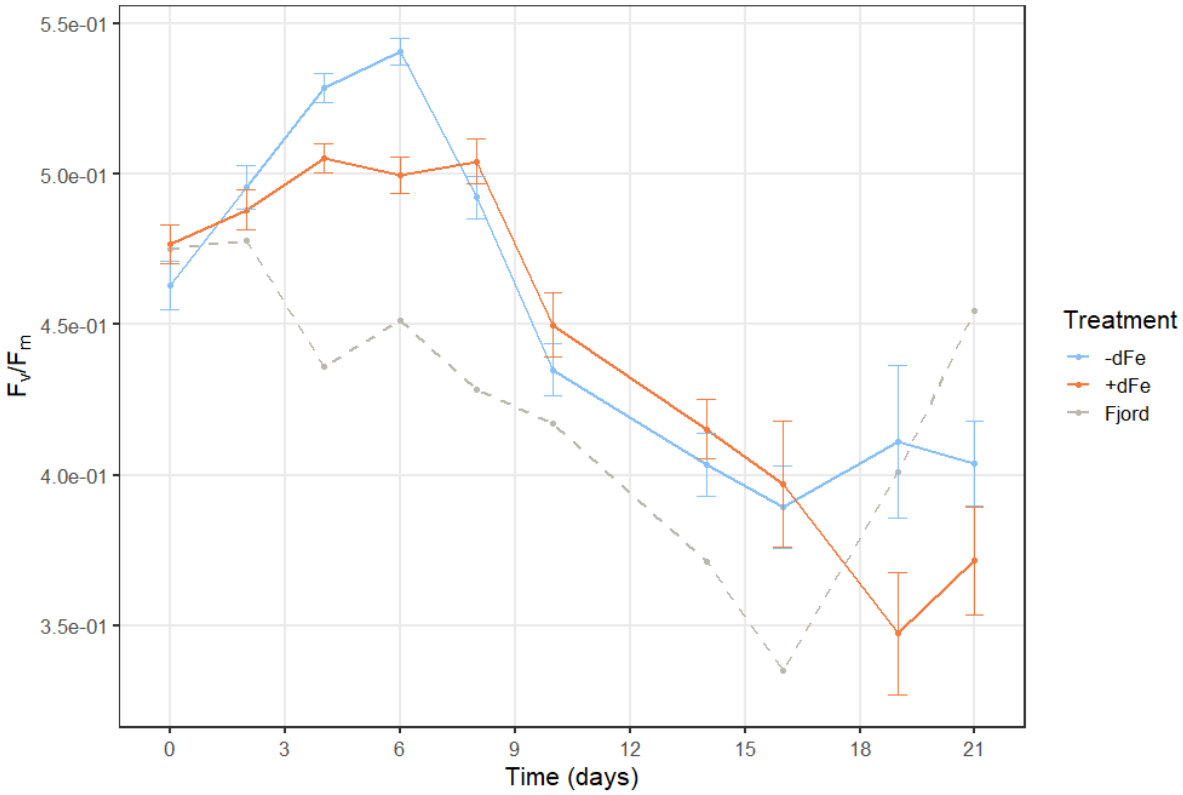

Figure A8. F_v/F_m mean values throughout the experiment for both the -dFe (blue line) and +dFe (orange line) treatments, and the fjord sample (dashed grey line). n=3 for day 0 and day 2 and n=6 for day 4 to day 21 for the -dFe and +dFe treatments, and n=1 for day 0 and day 2 and n=2 for day 4 to day 21 for the fjord.